Construction and Building Materials 520 (2026) 145989

Contents lists available at ScienceDirect

Construction and Building Materials

journal homepage: www.elsevier.com/locate/conbuildmat

Thermo-physical laboratory analyses of microencapsulated PCMs for thermal energy storage systems

Sara Franzè [a], Maria Chiara Dalconi [a], Filippo Agresti [b], Enrico Garbin [b], Simona Barison [b], Bernardo Cesare [a], Giorgia Dalla Santa [c,d], Antonio Galgaro [a,*]

[a] Department of Geosciences, Università degli Studi di Padova, Padova, Italy
[b] Institute of Condensed Matter Chemistry and of Technologies for Energy – National Research Council of Italy (ICMATE-CNR), Padova, Italy
[c] Department of Civil, Environmental and Architectural Engineering, Università degli Studi di Padova, Padova, Italy
[d] Department of Industrial Engineering, Università degli Studi di Padova, Padova, Italy

ARTICLE INFO

Keywords:
Thermal Energy Storage (TES)
Microencapsulated phase change materials (mPCM)
Cement mortar
Energy saving
Thermo-Active Building Systems (TABS)
Thermo-mechanical properties

ABSTRACT

This study investigates the integration of microencapsulated paraffin-wax Phase Change Materials (mPCMs) into cementitious mortars as an innovative Thermal Energy Storage (TES) strategy. Despite their environmental and cost benefits, incorporating mPCMs into mortar poses challenges, particularly in delivering suitable workability and mechanical properties. The research evaluates the impact of water-slurry mPCMs on TES performance in mortar samples with increasing mPCM concentrations. A comprehensive approach is employed to assess thermal properties under diverse conditions, using calorimetric, conductivity, and microthermometric methods. Mechanical and microstructural analyses provide insights into mPCMs' influence on cement matrices. The study examines how mPCMs affect various aspects of mortar, including compressive strength, microstructure, thermal conductivity and latent heat. The findings contribute to a deeper understanding of mPCM integration in cementitious binders for TES systems, addressing both thermal and mechanical behaviour. This research supports the development of sustainable heat storage solutions, advancing also more efficient and practical applications of mPCMs in structural building materials and TES systems.

1. Introduction

The increasing global demand for energy, driven by economic and population growth, has led to extensive reliance on fossil fuels, contributing to resource depletion and significant greenhouse gas emissions. To mitigate these impacts and meet sustainability goals, renewable energy sources such as solar, wind, geothermal, and hydroelectric are becoming increasingly integrated into the energy mix [1]. However, due to the climatic uncertainties, the means of storing renewable energies, often discontinuous and/or cyclic, has become urgent [2]. This has led to a need to develop efficient and sustainable methods of storing energy. Among them, Thermal Energy Storage (TES) plays a key role by storing energy in the form of heat for later use in heating, cooling or power generation applications [3–5]. TES can be categorized into three types: Sensible Heat Storage (SHS) [6,7] which is used heavily in Concentrated Solar Power (CSP) [8], Latent Heat Storage (LHS) [9] that include Phase Change Materials (PCMs) [10] and Thermochemical Storage (TcS) [11].

The application of Phase Change Materials (PCM) on Thermo Active Building Systems (TABS), also known as thermally activated building structures, is a significant research area aimed at enhancing the thermal inertia of buildings, shifting peak energy loads, and improving thermal comfort. Research shows that integrating PCM into TABS can lead to 20–40% energy reductions and 50% improved thermal storage compared to traditional concrete systems [12].

Latent Heat Storage (LHS) systems utilize PCMs that can release or absorb energy through changes in their physical state. The heat is primarily stored during the phase-change process at a relatively constant temperature, which is directly linked to the substance's latent heat. LHS offers two main advantages over Sensible Heat Storage (SHS): higher energy storage density and the ability to store heat within a narrow temperature range. Initially, PCMs in LHS systems behave similarly to materials in SHS systems, with temperature rising linearly as system enthalpy increases. However, during the phase change, heat is absorbed or released at a nearly constant temperature [5]. This work primarily focuses on PCMs derived from LHS systems. PCMs can be categorized based on their phase transformations: solid-solid, solid-liquid,

* Corresponding author.
E-mail address: antonio.galgaro@unipd.it (A. Galgaro).

https://doi.org/10.1016/j.conbuildmat.2026.145989
Received 3 December 2025; Received in revised form 13 March 2026; Accepted 15 March 2026
Available online 19 March 2026

Nomenclature

Abbreviations

TES	Thermal Energy Storage
SHS	Sensible Heat Storage
CSP	Concentrated Solar Power
LHS	Latent Heat Storage
PCM	Phase Change Material
TcS	Thermochemical Storage
PW	Paraffin Wax
PEG	Polyethylene Glycol
mPCM	Microencapsulated Phase Change Material
NPCM	Nanoencapsulated Phase Change Material
DSC	Differential Scanning Calorimetry
TCS	Thermal Conductivity Scanner
MTPS	Modified Transient Plane Source
SEM	Scanning Electron Microscope
SE	Secondary Electrons
mRS	micro-Raman Spectroscopy
PPM	Polychromatic Polarization Microscopy
S	Standard Sand
C	Cement
W	Tap water
W_d	Water dispersion

Latin letters

m	Mass [kg]
V	Volume [m3]
T	Temperature [°C]
ff	Flexural strength [MPa]
f_c	Compressive strength [Mpa]
F_f	Load applied [N]
l	Distance between supports [mm]
b	Square section of prism [mm]
c_p	Specific heat capacity [J/(kg·K)]

Greek letters

ρ	Density [kg/m3]
ΔH	Latent heat [J/g]
α	Thermal Diffusivity [m2/s]
e	Thermal Effusivity [Ws1/2/(m2·K)]
k	Thermal Conductivity [W/(m·K)]

liquid-gas, and solid-gas. While gas transformations offer significant energy storage per unit volume, PCMs involve substantial volume changes that are challenging to manage. In contrast, solid-solid and solid-liquid transformations are more practical for thermal energy storage systems due to their minimal volume change, typically less than 10%. This characteristic makes these types of PCMs particularly suitable for efficient and manageable thermal energy storage applications [13–15]. Depending on the type of material used, PCMs are further divided into organic, inorganic [16–19], and eutectic types [17,20–22]. This study focuses only on organic PCMs.

Organic PCMs can crystallize with little or no subcooling and maintain their latent heat and self-nucleating properties. They are non-corrosive, melt congruently (liquid and solid composition is identical), and do not experience phase segregation. Although they are mainly solid–liquid PCMs, some organic PCMs like polyalcohol and polyethylene are solid–solid [21]. Organic PCMs present two main challenges: poor thermal conductivity, ranging from 0.1 to 0.3 W/(m·K), and issues with shape stabilization. These materials often require encapsulation in plastic containers to maintain their shape and prevent leakage during phase transitions.

They are further classified into Paraffin Wax (PW) [23] and non-paraffin organic PCMs [24,25], including Polyethylene Glycols (PEGs) [26], fatty acids, and derivatives. Paraffin waxes are composed mainly of straight-chain n-alkanes (CH_3–(CH_2)–CH_3) and release a significant amount of latent heat during crystallization of the (CH_3)– chain, exhibiting solid-liquid phase transition. The melting point and latent heat of fusion increase with chain length. Paraffin shows an increase in the melting temperature as the number of chains is increased [27,28]. They are excellent storage systems, having extensive use in building with the latent heat of 200–220 J/g and heat capacity of 2.14 – 2.4 J/(g·K). Paraffin waxes possess several desirable properties for their use in TES systems. These include chemical inertness (stable below 500°C), safety, reliability, predictability, and cost-effectiveness. Additionally, paraffin waxes are non-corrosive and available in a wide temperature range (5–80°C), making them versatile for various applications [17]. However, some issues include moderate flammability and low thermal conductivity, necessitating large surface areas and high latent heat for efficient heat transfer during the freezing cycle.

To overcome these issues, encapsulation techniques have been developed to contain the PCMs, enhance compatibility with construction materials, and reduce leakage [29]. The encapsulation is categorized by the size of particles into macro (>1000 μm), micro (1 μm to 1000 μm) and nano (1–1000 nm) models. Although the microencapsulated Phase Change Materials (mPCMs) is the most used concept, nanoencapsulated Phase Change Materials (nPCMs) has an ever-increasing demand [30]. As a matter of fact, with a smaller capsule, a higher surface area to volume ratio of the material will be provided, which enhances the heat transfer. PCM encapsulation is widely used in building cooling systems, where air passes through flat containers of PCM [31].

Various approaches to prepare the organic encapsulated PCM as a new kind of TES medium have been extensively developed and can be manufactured to suit the desired properties [32]. For these reasons there are several studies about mPCMs, where choosing the combination shell/core is the most important point. The proportion of core material in the capsule is usually between 20% and 95% by mass. The microcapsules may consist on a single particle or clusters of particles. Paraffin wax is one of the most employed PCM in mPCMs systems [33,34].

Microencapsulated Phase Change Materials in slurry form represent a significant advancement in PCM technology. These slurries have gained increasing importance as heat transfer fluids and thermal energy storage media [35–37]. In recent years, the integration of PCMs into cementitious materials has emerged as a promising strategy to enhance the thermal inertia of building envelopes and promote energy efficiency [35,38,39]. Slurries containing microencapsulated phase change materials (mPCM) have vast potential applications in the construction industry, especially for cement mortar and concrete. These innovative materials can be used in thermal energy storage systems like pavements, slabs, or energy geostructures. Energy geostructures are multifunctional technologies that serve both structural and energy exchange purposes, offering advantages such as reduced costs, land use, increased energy efficiency, and lower environmental impact. Examples of energy geostructures include energy foundations such piles, walls, tunnels, and other geo-structural components integrated with ground heat exchangers. This technology is gaining widespread adoption worldwide. A comprehensive database-driven analysis of energy geostructures is presented in [40]. For energy geostructures to fulfill their dual function, the constituent material must provide high thermal exchange efficiency while meeting the required mechanical strength. However, incorporating PCMs into cementitious materials presents certain challenges. The most significant concern is the potential deterioration of mechanical properties, in relation to the percentage of mPCM [39,41].

Studies have shown that adding PCMs to mortar mixes can have varying effects on mechanical performance [42,43]. Notably, as the PCM content increases from 0% to 20%, a reduction in compressive strength of up to 51% has been observed [44]. Incorporating these materials in mortars can also alter their workability, microstructure [45] and thermal properties [46,47]. This trade-off between thermal benefits and mechanical integrity highlights the need for careful consideration when implementing PCM technology in binding materials.

This study is focused on the evaluation of microencapsulated water-slurry mPCMs addition (with a melting temperature of around 70°C) in mortars behaviour, voted to improve the TES performance. A variety of different experimental techniques were applied to deeply characterize a series of mortar samples prepared with different microencapsulated PCMs concentrations ranging from 0% to 15% by total weight of the mortar (corresponding to a nominal percentage of mPCM ranging from 0% to 3.82%). All measurements were conducted at the Department of Geosciences, Università degli Studi di Padova, except for the Differential Scanning Calorimetry (DSC) measurements, which were performed at the Institute of Condensed Matter Chemistry and Technologies for Energy – National Research Council of Italy (ICMATE-CNR).

The following properties have been performed:

- The thermal properties (thermal conductivity, thermal diffusivity, thermal effusivity) of samples under dry conditions, at room temperature (around 20 °C) and high temperature (around 80–90 °C), were analysed with three devices: the Differential Scanning Calorimetry (DSC) [48], Thermal Conductivity Scanner (TCS) [49] and with Modified Transient Plane Source method (MTPS) [50].
- The mechanical properties of all specimens with different mPCMs ratios were also investigated by Compressive strength (f_c) [51] and Flexural strength (f_f) tests.
- Microstructures also were analysed with Scanning Electron Microscope (SEM) [52], polarized conventional (mineralogical) optical microscopy and polychromatic polarization microscopy [53]. Furthermore, micro-Raman Spectroscopy (mRS) [54] was employed to assess the distribution of mPCMs in the matrix.

Despite growing research on PCMs in construction materials, the specific application of mPCMs in slurry form mixed within cement mortars as a heat and energy storage medium has not been adequately addressed. While previous studies have extensively investigated the incorporation of PCM into cementitious materials, the majority of existing research has focused on low temperature PCMs intended for indoor thermal comfort and energy-efficient buildings. Most of these studies consider dry mPCMs, in contrast, fewer investigations have explored mPCM slurries. This study aims to further investigate the incorporation of mPCM slurry into cementitious mortars through a multidisciplinary experimental approach. Building upon existing literature, the work extends previous studies to mPCMs with higher phase transition temperatures and allows a combined evaluation of microstructural, thermal and mechanical behaviour in order to assess the feasibility of this approach for thermal energy storage applications.

In particular, the novelty and originality of this work lie in three main aspects. First, the study investigates a paraffin wax microencapsulated PCM system characterised by a medium temperature phase transition (around 70 °C), which is higher than the temperature ranges typically addressed in cementitious PCM composites for building comfort applications. Second, the mPCMs are incorporated in the form of an aqueous slurry rather than as dry microcapsules, allowing the investigation of mPCM slurries effects on mix design, density, porosity, mechanical performance and thermal transport properties. Third, an integrated and systematic experimental approach is adopted, combining complementary techniques including differential scanning calorimetry, thermal conductivity measurements at both ambient and elevated temperatures, mechanical testing, micro-Raman spectroscopy and scanning electron microscopy to establish correlations between microstructure, thermal behaviour and mechanical response. This combined perspective provides new insights into the feasibility and limitations of mPCM slurries incorporation in cementitious mortars for thermal energy storage applications.

This paper firstly presents the comprehensive experimental program in all the different applied measuring techniques and, secondly, the obtained results are presented and discussed.

2. Experimental program

2.1. Tested materials

The utilized PCMs are microencapsulated phase change materials, purchased from the company MikroCaps (https://www.mikrocaps.com/). These mPCMs, described in Table 1, are an aqueous suspension (water-slurry) of microencapsulated paraffin wax, with a membrane made of melamine-formaldehyde. A Portland Limestone Cement CEM II/B-LL 42,5 R, from Italcementi HeidelbergCement Group, was used to prepare the mortar samples. The phase composition of the cement and the grain size distribution are reported in Table 2. The phase composition was determined by quantitative phase analysis of x-ray powder diffraction data using the Rietveld method and the chemical composition by XRF analysis. Grain size distribution was measured by laser granulometry dispersing the powder sample in air, obtaining $D_{10} = 1.8$ μm; $D_{50} = 7.5$ μm and $D_{90} = 25.9$ μm. The cement estimated bulk density is 3031 Kg/m^3. The mortar used in this study contained standard Sand (S) certified in accordance with EN 196–1 and conforming to ISO 679:2009, purchased from Société Nouvelle du Littoral (https://standard-sand.com/). S is a natural sand, which is siliceous particularly in its finest fractions. Tap water (W) was also added following the standard guidelines (EN 196–1).

2.2. Methodology

2.2.1. Sample preparation

The experimental program was prepared to investigate the physical and mechanical properties, thermal conductivity, heat transfer evolution and the microstructures of the mPCM-mortars mix. To do this, five different compositions were prepared in the form of 25 initial samples of different shapes to conduct various analyses. The compositions were standard mortar without mPCMs (Ref. mix 0% mPCM+S) and four mixtures of mortar with different mPCMs contents (Mix 8.0% mPCM+S, Mix 10.6% mPCM+S, Mix 11.9% mPCM+S, Mix 14.6% mPCM+S). In this study, the mPCM content is primarily expressed as the mass fraction of mPCM slurry with respect to the total mortar weight, as this represents the experimentally controlled parameter during sample preparation. The corresponding nominal PCM content is also reported, derived from the known PCM concentration in the slurry, in order to facilitate comparison with previous studies. In detail, Table 3 shows the mixing percentages of the mortars with mPCMs for all samples. The mortar specimen was prepared in the laboratory with a fixed cement/sand ratio

Table 1
Technical data of MikroCapsPCM70 slurry.

MikroCapsPCM70-slurry	Data sheet
PCM content in the dispersion	30%
PCM content in dry capsule	75–80%
Dry content in the dispersion	36%
PCM melting area	68–73 °C
Heat storage capacity (of slurry)	60–78 J/g
Heat storage capacity (of dried microcapsules)	> 170 J/g
pH	7,0–9,0
Density	900–970 g/L
Viscosity (at 25 °C)	10–1000 cPs
Appearance	White slurry
Average particles size	2–20 μm

Table 2
Phase composition and chemical composition of CEM II/B-LL 42,5 R.

Phase	wt%	esd	Oxide	wt%
Alite – C3S	40.7	0.3	**SiO_2**	14.8
Belite – C2S	10.5	0.3	**Al_2O_3**	3.1
C3A	2.0	0.2	**Fe_2O_3**	4.9
C4AF	12.3	0.3	**CaO**	70.8
Calcite	28.5	0.2	**MgO**	1.4
Gypsum	0.8	0.1	**SO_3**	3.3
Bassanite	2.8	0.1	**P_2O_5**	0.2
Anhydrite	1.1	0.1	**K_2O**	0.8
Quartz	0.5	0.1	**Na_2O**	0.4
Portlandite	0.9	0.1	**LOI**	15.0

of 1:3. For the control sample, a fixed water-to-cement ratio (w/c) of 0.50 was employed. In the four samples containing mPCM, the addition of free water to the mixtures was progressively reduced resulting in a w/c ratio ranging from 0.35 to 0.30 as the mPCM content increased. The w/c ratio was calculated considering only the free water added to the mixtures, while the nominal ratio accounted for the free water and the water content present in the mPCM slurry. This slurry had a dry content of 36%, with PCM (paraffin wax) constituting 30% of the total slurry weight. For samples with mPCM content exceeding 9.3%, additional free water was introduced to enhance the mixture's workability. This modification was necessary because maintaining a constant nominal water content in samples with high mPCM concentrations resulted in rigid and unworkable pastes, unsuitable for practical applications. The proportional increase in water content allowed for consistent paste workability across all samples. No other additives were used to improve workability. It is well established in the literature that mPCM incorporation significantly alters the rheology of cementitious mixtures beyond what a simple slump value can capture [55]. The mPCM particles, due to their water-absorbing shell surfaces and the increased solid volume fraction they introduce, raise both the yield stress and the plastic viscosity of the paste, resulting in higher water demand to maintain equivalent workability [56,57]. The progressive increase in free water added to the mixtures was therefore a deliberate design choice aimed at maintaining consistent workability across all compositions. The consequent trade-off between workability and compressive strength is well documented for mPCM-mortar systems [58], and the mechanical results obtained in this study are fully consistent with this expected behaviour.

The mixing process for ref. mix 0% mPCM+S sample was conducted as follows: the water was mixed with cement for 1 min using a vertical shaft stirrer set at a speed of 300 rpm, subsequently sand was added to the mixture and mixed for another minute. In the samples containing mPCM, water and mPCM were mixed with cement for 1 min; after this, sand was added to the mixture and mixed for another minute. The moulding procedure was identical for all samples. The mortar paste was poured into the mould up to halfway and shaken with 30 strokes. Subsequently, the mould was filled to the brim, regularized, and shaken with another 30 strokes. For the curing process, samples were left in a curing cabinet maintained at 20 ± 1°C and humidity from 95% to saturation. After 28 days, specimens were demoulded and smoothed using sandpaper.

A total of 25 samples were prepared, five for each composition. Five samples (one per composition), measured 6.5 cm× 5 cm x 4.5 cm (Fig. 1a), were used for thermal conductivity measurements (with MTPS at 20°C and 80°C), micro-Raman analysis, and DSC analysis. The remaining 20 samples (four per composition), measured 1.5 cm x 1.5 cm

Table 5
Density of mPCM and mixed mortars samples with mPCMs, depending on nominal amount of PCM and water/cement ratio.

Mix ID	Nom. PCM [%]	Nom. W/C	Bulk Density [kg/m^3]
Ref. Mix 0% mPCM+S	0.00%	0.50	2160.26
Mix 8.0% mPCM+S	2.30%	0.57	2053.12
Mix 10.6% mPCM+S	2.94%	0.59	2019.68
Mix 11.9% mPCM+S	3.25%	0.61	2006.30
Mix 14.6% mPCM+S	3.83%	0.70	1922.32
mPCM	100%	/	950.00

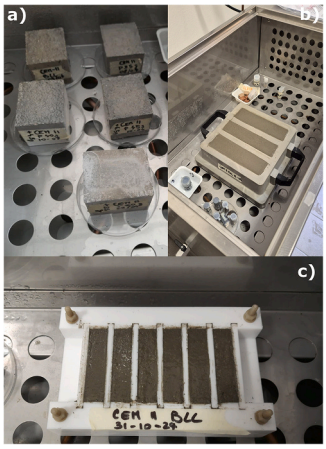

Fig. 1. a) Samples (6.5 cm×5 cm x 4.5 cm) used for thermal conductivity measurement with MTPS, micro-Raman and DSC; b) Samples of size 1.5 cm× 1.5 cm× 6 cm used for compressive strength tests, SEM and thermal conductivity measurements with TCS; c) Samples prepared according to EN 196–1:2016 (E) of size 4 cm× 4 cm x 16 cm used for flexural and compressive strength tests.

Table 3
Proportions of the 25 mixed mortars samples with mPCMs.

Mix ID	C [g]	S [g]	W [g]	mPCM slurry [g]	mPCM slurry %	W/C	Nom. PCM [g]	W_d [g]	Nom. W/C	Nom. PCM %
Ref. Mix 0% mPCM+S	137.50	412.50	68.75	0.00	0.00%	0.50	0.00	0.00	0.50	0.00%
Mix 8.0% mPCM+S	137.50	412.50	48.13	48.13	8.05%	0.35	14.44	30.80	0.57	2.30%
Mix 10.6% mPCM+S	137.50	412.50	43.28	61.88	10.43%	0.31	18.56	39.60	0.60	2.93%
Mix 11.9% mPCM+S	137.50	412.50	41.25	68.75	11.63%	0.30	20.63	44.00	0.62	3.25%
Mix 14.6% mPCM+S	137.50	412.50	44.75	82.50	13.87%	0.33	24.75	52.80	0.71	3.82%

Table 4
Proportions for the mixed mortars samples (4x4x16 cm) with mPCMs.

Mix ID	C [g]	S [g]	W [g]	mPCM slurry [g]	mPCM slurry %	W/C	Nom. PCM [g]	Wd [g]	Nom. W/C	Nom. PCM %
Ref. Mix 0% mPCM+S	450.00	1350.00	225.00	0.00	0.00%	0.50	0.00	0.00	0.50	0.00%
Mix 14.6% mPCM+S (+W)	450.00	1350.00	121.50	270.00	14.05%	0.27	81.00	172.80	0.65	3.87%
Mix 14.6% mPCM+S (++W)	450.00	1350.00	146.25	270.00	13.87%	0.33	81.00	172.80	0.71	3.82%

x 6 cm (Fig. 1b), were used for compressive strength tests, for SEM, for thermal conductivity measurements (with TCS at 20 °C). This set of small size specimens were intended for conducting several tests to optimize the mixtures while limiting the amount of material to be used. Once the optimal mPCM content and relative w/c ratio for the mixtures were determined, larger mortar samples complying with EN 196–1–1:2016 were prepared to characterize the mechanical properties of specimens with conventional mortar sizes. The additional samples were prepared for two compositions: the reference mix (0% mPCM+S) and mortar with the maximum mPCM concentration of 14.6% (Mix 14.6% mPCM+S) (Table 4). The samples named +W and + +W have been prepared by adding an additional amount of water to improve workability. They were cast in moulds consisting of three horizontal compartments, allowing for the simultaneous preparation of three prismatic specimens. Each specimen measured 4 × 4 cm^2 in cross section and 16 cm in length (Fig. 1c). After curing for 2 days, the specimens were demoulded and cured for an additional 26 days. Then, the specimens were measured and tests were conducted to determine their flexural and compressive strengths.

2.2.2. Bulk density measurements

After 28 days of curing, the specimens were regularised by lapping with abrasive agents or sandpaper. The bulk density ρ of all samples was determined by measuring their volume V and their mass m independently at room temperature (i.e., $\rho = m/V$).

2.2.3. Mechanical tests

Tests were performed on mortars cast in 6 × 1.5 × 1.5 cm^3 moulds, after 28 days of curing, utilizing the Uniframe 70-T1192–Controls press, an electromechanical press designed for force and displacement-controlled load testing. These were the preliminary screening tests, from which the most promising mixture was selected for subsequent full standard testing. A load cell with a maximum capacity of 25 kN was used to conduct tests at a displacement speed of 0.6 mm/min. The compression tests were performed using a scaled equipment developed at the CIRCe Center (University of Padua) by the 4th author and already used in previous research on cementitious materials [59]. Following the standards, 6 tests were conducted for each composition and the compressive average values with related Coefficient of Variation (CoV) were calculated.

Subsequently, tests were carried out on standard 4 × 4 × 16 cm samples (after 28 days of curing) to measure flexural and compressive strengths, according to EN 196–1. Measurements were performed applying a loading rate of 2400 N/s for compressive strength and 50 N/s for flexural strength [60].

Finally, the compressive strength and flexural strength (f_f) were calculated for the 4 × 4 × 16 cm^3 specimens, according to EN 196–1 standard [60]. f_f in this case was calculated as:

$$f_f = \frac{1.5 \bullet F_f \bullet l}{b^3} \quad (1)$$

Where f_f is the flexural strength, b is the side of the square section of the prism, F_f is the load applied to the middle of the prism at fracture and l is the distance between the supports. The 9 specimens (3 of ref. mix 0% mPCM+S and 6 of mix 14.6% mPCM+S) were broken at 28 days of curing.

2.2.4. Microstructural analysis

2.2.4.1. Micro-Raman spectroscopy (mRS). The distribution of mPCMs within the cement matrix was analysed using a Witec alpha 300 R confocal Raman micro-spectrometer. The analysis was conducted with a laser wavelength of 532 nm, a nominal laser power of 10 mW. The spectrometer was equipped with a grating of 300 g/mm. The mPCMs used in this study were made of paraffin wax, which exhibits a diagnostic Raman band at 2885 cm^{-1}.

To obtain an overview of the mPCM distribution, maps were acquired covering an area of 250 x 180 microns. The mapping resolution was set to 50 points per line and 40 lines, with step size of 5 microns along the X-axis and 4.5 microns along the Y-axis. Multiple areas were selected in the bottom and top zones of the samples, relative to the casting direction. The maps were acquired in 'scan' mode with an integration time of 1 s and a laser scan rate of 50 s/line. Each mapping session had a total duration of 35 min.

2.2.4.2. Polarizing and polychromatic polarization microscopy (PPM). In order to visualize the behaviour of paraffin wax crystals within the microcapsules before and after the phase changes, optical microscopy of mPCMs was performed with different instruments and techniques. Conventional transmitted polarized light (petrographic) microscopy was performed using a Zeiss Axioscop 40pol at ambient temperature with small amounts of sample on glass slides, and with a Zeiss Photomicroscope III for samples studied in the heating-freezing stage. Ambient temperature observations were made also using the novel PPM technique [53] which allows detection and analysis of materials with very low birefringence.

2.2.4.3. Microthermometry. Microthermometric analysis of mPCM was performed using a heating - freezing stage installed on a polarizing microscope. The stage is a Linkam THMS600, with an operating range of −195 °C to + 600 °C; it enables direct optical observations of the phase changes occurring within mPCMs, i.e., melting during heating and crystallization during cooling. It also allows precise determination of melting temperatures with an uncertainty of 0.2 ° C. The apparatus is electronically controlled for heating/cooling rates and is equipped with a camera (Moticam 580, 5.0 MP) capable of filming the ongoing experiment in real time. Samples of mPCMs were dried on a sample holder and subjected to 30 heating-cooling cycles inducing melting and crystallization. It should be noted that, hereafter, the term "dry mPCM" refers to a sample of mPCM slurry that was dried at ambient temperature for at least 48 h prior to testing. Whereas "wet mPCM" denotes the mPCM slurry in its as-received condition, i.e. in the liquid state as supplied by the manufacturer and used directly without any drying treatment. The dry mPCM slurry was observed before and after the cycles for a comparison of its microstructures.

2.2.4.4. Scanning electron microscope (SEM). SEM images were acquired using a FIB-FE-SEM Tescan SOLARIS microscope. Two specimens were selected for initial analysis: one from the reference mix 0% mPCM+S and one from the mix with 14.6% mPCM+S. These specimens were taken from samples that had undergone compressive strength testing at 28 days but had not received any heat treatment. They were embedded in epoxy and polished to obtain a flat surface sample. Carbon coating was applied to the sample surface prior to SEM analysis.

Following the Differential Scanning Calorimetry (DSC) tests, additional samples were analyzed. These included the reference mix 0% mPCM+S, the mix with 11.9% mPCM+S, the mix with 14.6% mPCM+S, and a single dry mPCM sample that had been heat-treated. For comparison, a sample of dry mPCM that had not undergone thermal alteration was also included in this analysis. For the Scanning Electron Microscopy (SEM) preparation, the post-DSC samples were fragmented, dispersed on carbon tape, and coated with chromium.

2.2.5. Differential scanning calorimetry (DSC)

DSC measurements were conducted using a DSC Mettler Toledo DSC3 with 40 microlitre aluminium crucibles. The heating rate was set to 5 °C/min within a temperature range of 30 ± 5 °C to 90 ± 5 °C. Samples of dry mPCM, wet mPCM, ref. mix 0% mPCM+S and all concentrations of mPCM-mortar mix were analysed. For these latter samples, heating and cooling cycles were performed on three different

portions of the same sample, taking material from the top, middle and bottom respectively, as shown in Fig. 2. Finally, in the mPCM slurry, in the ref. mix 0% mPCM+S and in the central section of the samples containing mPCM-mortar mixes, 30 consecutive heating and cooling cycles were performed between 30 °C and 95 °C at 5 °C/min.

2.2.6. Thermal conductivity tests

As for the thermal properties' measurements, two devices have been used: the TCS to measure thermal conductivity and diffusivity at room temperature (20°C); and MTPS to measure thermal conductivity and effusivity at room temperature (20°C) and at high temperature (80–85°C).

2.2.6.1. Thermal conductivity scanner (TCS). Thermal Conductivity (*k*) was monitored by means of a thermal conductivity scanner (TCS) that is able to measure *k* together with thermal diffusivity (α) on solid materials like rock samples or cements. The TCS uses the optical scanning technology developed by Yuri Popov [61]. The optical scanning technology is based on scanning a sample surface with a focused, mobile and continuously operated optical heat source in combination with infrared temperature sensors. The determination of the thermal properties of the analysed materials is based on the comparison with temperature differences measured on two standard samples labelled A and B (certified samples having known thermal properties).

TCS has an optical scanning method that has an accuracy and precision of 3% for *k* and 5% for α, scanning speed of 5 mm/s and a measurement range for *k* from 0.20 to 25.00 W/m·K and for α from 0.6 to 3.0 mm^2/s. Before the measurement, samples were prepared by painting surfaces to be analysed with acrylic black paint to avoid reflection during measurement (a scanning line with a width of at least 2 cm). Used standards have *k* values of 1.35 W/(m·K) (sample A) and 6.41 W/(m·K) (sample B) and α values of 0.850 mm^2/s (sample A) and 2.750 mm^2/s (sample B). Thermal conductivity *k* and thermal diffusivity α were calculated by comparing the temperature of the measured sample with the temperature of the reference standards.

2.2.6.2. Modified transient plane source method (MTPS). Thermal conductivity (*k*) and thermal effusivity (*e*) measurements were performed using a thermal conductivity analyser (C-Therm), under standard room temperature or high temperature (80–85 °C) and atmospheric pressure conditions [62]. The instrument uses the MTPS technique, which involves a one-sided heat reflectance sensor that briefly applies a constant heat pulse to the sample. The voltage change across the sensor is recorded during the measurement as its temperature increases slightly due to the applied pulse. The pulse duration is short enough to assume the sensor is in contact with an infinite or semi-infinite solid. The measurement time is selected to ensure that the boundaries of the sample do not significantly impact the sensor's temperature rise.

The flat surfaces of the specimens were covered with a thermal paste to ensure continuity of contact with the sensor and minimise thermal resistance. Thermal conductivity and effusivity were measured directly, with precision within 1% relative standard deviation (RSD) and accuracy within 5%. The instrument was used both to perform measurements at room temperature and at rising temperatures (up to a maximum of 80–85 °C) by inserting the sample and the sensor inside an oven (Memmert GmbH - UF55 Plus) with forced air circulation. Before starting sample measurements, a reference material test must be run for calibration. A specific reference material is chosen according to the characteristics of the sample and the expected thermal conductivity values. The Pyroceram reference material was used for this set of measurements. The specifications for the reference materials provided with the instrument are outlined in the manual [50].

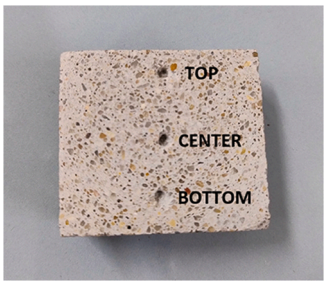

Fig. 2. Sampling areas for DSC analysis.

3. Results and discussion

The results of the different methods explained earlier are presented and discussed herein.

3.1. Bulk density

The incorporation of mPCMs in mortars results in a slight decrease in their bulk density, as shown in Table 5. The data indicates that adding mPCM slurry up to a concentration of 14.6% within the mortar leads to a density reduction of approximately 11% compared to the reference mix 0% mPCM + S. This observed trend can be attributed to the lower density of mPCM relative to cement and sand, and it aligns with findings reported in previous studies [63,64]. In addition, the use of mPCMs in slurry form introduces an extra amount of water into the mixture, which increases the effective porosity of the mortar, further contributing to bulk density reduction [65]. It is important to note that the addition of mPCM slurry introduces extra water into the system, thereby increasing the nominal water-to-cement ratio (as shown in Table 2 and Table 4). The combined effect of the lower intrinsic density of the mPCMs and the increase in porosity associated with the higher nominal w/c ratio explains the progressive decrease in bulk density with increasing mPCM content [66]. As expected, the bulk density values exhibit an inverse correlation with the nominal w/c ratio values, which is illustrated in Fig. 3.

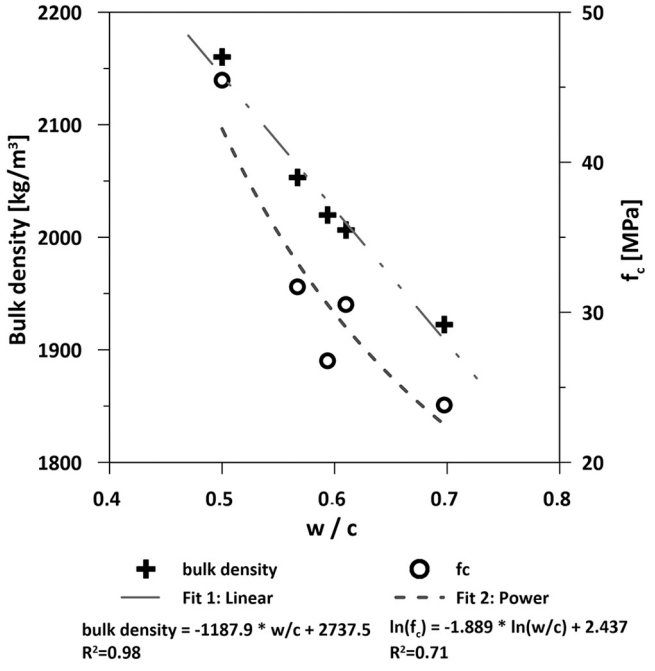

Fig. 3. Samples bulk density and compressive strength (f_c) as a function of the water to cement ratio, together with the fitting curves. The decreasing trend reflects the combined effect of increasing mPCM content and higher nominal water-to-cement ratio.

3.2. Compressive strength and flexural strength

To examine the impact of the mPCMs slurry addition fraction on the mechanical properties, specimens with different mPCMs portions were tested. Table 6 presents all the compressive strengths and flexural strengths results (represented also in Fig. 3). Flexural strength values are reported only for EN 196–1 standard prisms, as flexural tests were not performed on smaller samples. All specimens, with different mPCM percentages (0%, 8,0%, 10,6%, 11,9% and 14,6%), were cured for 28 days.

Test results show that the compressive strength value of mortar specimen with mPCMs was lower than that of the reference Mix 0% mPCM+S (i.e., 0% mPCMs) having a strength of 45.5 MPa at 28 days of curing. This compressive strength decreased from 31.7 MPa (Mix 8.0% mPCM+S) to 23.8 MPa (Mix 14.6% mPCM+S), with a reduction ranging from 30.3% to 47.7%, consistent with the findings of previous works [67]. The compressive strength further decreased when the mPCMs ratio was increased, with the exception of Mix 11.9% mPCM+S, probably due to an influence of the operator's handling during sample preparation. As expected, mortars with lower water to cement ratio (W/C) had higher compressive strength.

The 6 samples with mPCM have two different water concentrations, 3 reflect the same water content as the smaller samples, while 3 others have a reduced water concentration. It is observed that in the larger samples, the workability of the material increased and the amount of water could be reduced as the mPCM concentration increases.

Also, in these ref. mix 0% mPCM+S samples, what was observed for the smaller specimens is confirmed with an average compressive strength value of 47.4 MPa and an average value of 6.0 MPa for flexural strength. For the sample mix 14.6% mPCM+S, on the other hand, the same average compressive strength value of approximately 23.5 MPa and an average flexural strength value of 4.1 MPa were maintained (for the sample with the highest water content). For the others with reduced water content, the average compressive strength value was 28.3 MPa and 4.9 MPa flexural strength, confirming that reducing the water content in the mix results in higher compressive strength values. Nonetheless, the presence of the mPCM always hinders the overall strength of the sample.

PCMs have low shear strength and stiffness compared to cement and some PCM particles fail during loading. In addition, the bond between the mPCMs and mortar components is weak, reducing the mortar's mass loss and compressive strength [68]. In the literature, however, an increase in compressive strength over time is reported for the same mPCM content [63]. This observation indicates the retarding effect of the mPCMs addition on the cement hydration process. The delay in hydration reactions was previously evidenced in other types of PCM inclusion as well [69] and it is reasonably correlated with the breakage of some microcapsules as also observed in our SEM analyses.

According to the EN 196–1:2016 standards for mortar classification, the compressive strength and flexural strength was considered in this work [70]. The mechanical characterization reveals a systematic deterioration in compressive strength with increasing mPCM content, with reductions ranging from 30.3% to 47.7% compared to the reference mixture (45.5 MPa). This progressive strength decline can be attributed to three synergistic mechanisms: (i) the inherently low mechanical properties of the PCM phase, (ii) weak interfacial bonding between mPCMs and the cementitious matrix, and (iii) increased porosity resulting from slurry incorporation. The water-to-cement ratio optimization study demonstrates that, while increased mPCM content enhances workability, the net effect on compressive strength remains negative. Optimizing W/C ratio can partially mitigate strength loss (from 23.5 MPa to 28.3 MPa for Mix 14.6%), though values remain substantially below the reference (47.5 MPa), indicating that fundamental mechanical limitations imposed by mPCM incorporation cannot be fully overcome through mix design adjustments alone.

The compressive strength obtained for the mortar with mPCMs specimens proves their potential in different architectural applications and potential thermal energy storage capabilities. In fact, the consistency between small and standard specimens validates the scalability of observations. Despite the mechanical compromise, residual compressive strengths (23.5–31.7 MPa) remain within acceptable ranges for non-structural applications, confirming the feasibility of these materials for thermal energy storage in architectural contexts where moderate mechanical performance is sufficient. Similar results were reported for the different mortar rates with mPCMs [67].

3.3. Microstructure analysis

3.3.1. Micro-Raman spectroscopy (mRS) of cement mortar with mPCMs

The spatial distribution of mPCMs through the cement matrix was investigated by mapping the characteristic Raman band of paraffin wax at 2885 cm^{-1}. This analysis was conducted in selected areas within both the top and bottom zones of mortar sample 14.6% mPCM+S. This selection of mapping locations was designed to investigate potential segregation effects of the mPCMs within the mortar matrix. The rationale behind this approach stems from the fact that mPCMs have a lower density compared to cement phases, and the microcapsules might accumulate in the upper portion of the freshly cast mortar paste before the setting process begins.

Fig. 4 presents an example of full Raman spectra obtained from the 14,6% mPCM + S sample, the mPCM slurry and the reference mortar. The peak corresponds to the maximum intensities of the 2885 cm-1 band, which is diagnostic for paraffin wax. Upon comparing the top and bottom zones of the sample, no significant differences were observed. This suggests that, within the limitations of the small areas investigated, there are no detectable segregation effects of the mPCMs in the mortar matrix. Micro-Raman spectroscopy has been previously employed to investigate phase identification and spatial distribution in cementitious materials and PCM-based systems, demonstrating its suitability for the analysis of heterogeneous composites [71–73]. However, to the authors' knowledge, this is the first study applying micro-Raman mapping to cement mortars incorporating mPCMs in slurry form and specifically targeting a PCM with a phase transition temperature of approximately 70 °C, providing new insights into capsule distribution

Table 6
Compressive strengths (f_c) and Flexural strengths (f_f) results for the mixed mortar samples. The coefficient of variation is reported in brackets. Flexural strength (f_f) values are reported only for EN 196–1 standard prisms.

Mix ID	Samples dimension [cm]	Curing days	Bulk Density [kg/m^3]	f_c [MPa]	f_f [MPa]
Ref. Mix 0% mPCM+S	1.5×1.5×6	28	2160 (0.5%)	45.5 (12.7%)	/
Mix 8.0% mPCM+S	1.5×1.5×6	28	2053 (0.5%)	31.7 (6.1%)	/
Mix 10.6% mPCM+S	1.5×1.5×6	28	2020 (0.3%)	26.8 (4.4%)	/
Mix 11.9% mPCM+S	1.5×1.5×6	28	2006 (0.2%)	30.5 (4.5%)	/
Mix 14.6% mPCM+S	1.5×1.5×6	28	1922 (0.6%)	23.8 (4.3%)	/
Ref. Mix 0% mPCM+S	4×4 x 16	28	2223 (0.3%)	47.5 (8.7%)	6.05 (4.5%)
Mix 14.6% mPCM+S (+W)	4×4 x 16	28	2018 (1.2%)	28.3 (4.0%)	4.97 (27%)
Mix 14.6% mPCM+S (++W)	4×4 x 16	28	1993 (1%)	23.5 (4.0%)	4.09 (26%)

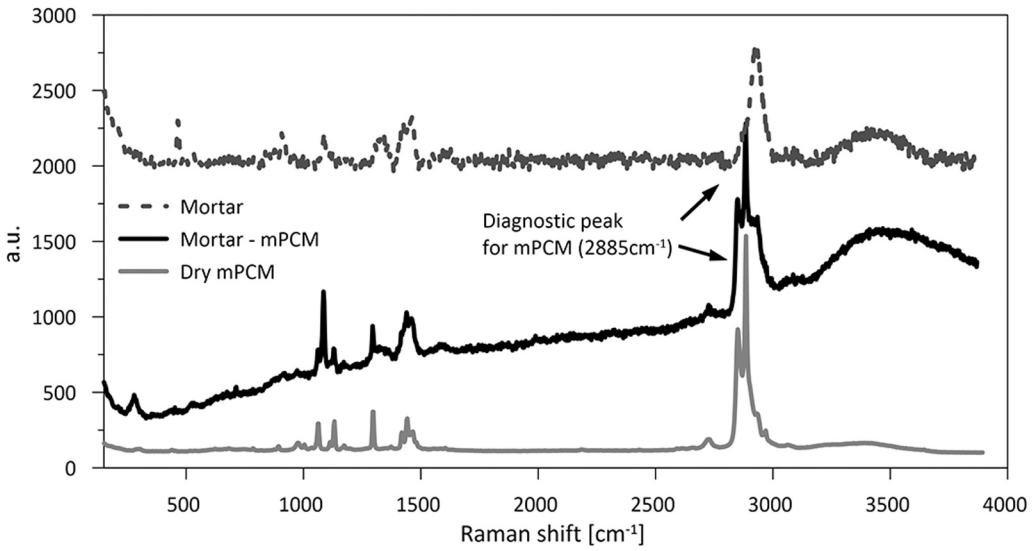

Fig. 4. Representative Raman spectra of ref. mix 0% mPCM + S, dry mPCM and mix 14.6% mPCM + S. In the dotted spectrum a peak at 2927 cm-1 is present, which is likely due to contamination from organic material (e.g. glue).

and stability under these conditions.

3.3.2. *Microthermometry and optical microscopy observations*

Dry mPCMs were then observed at ambient temperature with a polarizing microscope to see their original shape before and after melting events (Fig. 5). Portions of the sample were chosen in which the microcapsules were clearly visible and rather isolated, in order to observe both the capsule morphology and the crystalline phases of the inner paraffin wax in the solid state. The latter can be easily identified by their variable interference colours under crossed-polarization mode (Fig. 5a). Various objectives (20x, 50x and oil immersion 100x) were used to acquire images of the sample.

Afterwards, a series of videos and photomicrographs of the same pre-selected portion of the sample were taken during heating/cooling cycles in the Linkam THMS600. Four pre-cycles of heating and cooling images were taken, two at 60 °C, in the solid crystalline state and two at 75 °C, in the completely melted state of the paraffin wax of the mPCMs. Movie (supplementary material 1 - video) enables visualization of the melting of the paraffin wax by the sudden disappearance of the optically anisotropic material contained within the microcapsules' membrane. Melting of the paraffin wax took place in the temperature range 71 °C - 74 °C. Thirty heating/cooling cycles were performed, and photos were then captured on the same area (Fig. 5b). Subsequently, more detailed and magnified images of the same sample (post cycles) were acquired at the ZEISS optical microscope, also under PPM mode (Fig. 5c).

Supplementary material related to this article can be found online at doi:10.1016/j.jallcom.2022.164017.

Optical microscopy also shows that the shape of microcapsules at ambient temperature is often not perfectly spherical, with frequent buckling of the shells, that is more apparent in the larger capsules (Fig. 5d) but is widespread at all sizes. Shell buckling is a well-known type of deformation of micro- and nanocapsules [30] and is probably due to the internal depressurization microcapsules undergo in response to the volume contraction (approximately 15% [74]) related to the liquid/solid transition (crystallization of the paraffin wax). After the 30 heating and cooling cycles, microcapsules were brought up to 95 °C to check for any damages at elevated temperatures. Optical microscopy did not show any noticeable changes.

From these observations and comparisons of the same sample, analysed before and after the heating and cooling cycles, no major changes in the microcapsules are observed. Microcapsules seem to retain their structure and do not suffer damage after the thermal cycles performed on the sample. The solid paraffin wax consists of aggregates of sub-micrometric crystals, which are particularly evident in the coarser spherules and under PPM imaging (Fig. 5e and Fig. 5f).

3.3.3. *Scanning electron microscopy (SEM) of cement mortar*

SEM images of the polished sections of the reference mortar and mortar with mPCM samples are presented in Fig. 6. The mortar sample containing mPCM exhibits numerous circular voids with a maximum diameter of approximately 15 μm. These voids are attributed to both the PCM microcapsules and air bubbles entrapped in the mortar paste during mixing. The stabilizing agents in the mPCM slurry likely caused a mild foaming effect. This increase in spherical voids is consistent with the reduction in bulk density observed for mPCM-containing mortars and contributes to the modification of both mechanical and thermal properties. Notably, the mPCMs appear to be well-distributed throughout the cement matrix, without clustering in specific areas. Furthermore, no apparent damage is observed in the interfacial transition zones surrounding the mPCMs. This homogeneous distribution confirms that segregation effects are limited, in agreement with the results obtained by micro-Raman mapping.

The almost spherical geometry of the voids in mortar sample is consistent with the morphology of the mPCMs used (see Figs. 7a, 7b). The outer shell surface of the mPCMs, in the majority of cases, has no damage or rupture, confirming that the mPCMs are suitable to resist the mixing, casting process, curing, heating and cooling cycles and ensure good binder-PCMs integrity [67]. Similar SEM observations, highlighting intact microcapsules and good dispersion within the cement matrix, have been reported in previous studies on cementitious mortars incorporating microencapsulated paraffin PCMs, confirming the suitability of SEM for investigating PCM–matrix interactions [75–77]. A good connection exists between the different material constituents of the ref. mix 0% mPCM+S and homogeneous distribution in their matrix with different contents of PCMs.

Samples that underwent thermal treatment via DSC (30 heating and cooling cycles from 35 °C to 95 °C at a rate of 5 °C/min) were analysed. The compared samples included mPCMs in its dry form, shown in Figs. 7c, 7d (contrasted with its non-thermally treated counterpart) and sample mix 14.6% mPCM+S, shown in Figs. 7e, 7f). It is observed that the thermally untreated microcapsules exhibit a more well-defined spherical shape. Additionally, a noticeable size variation is observed, ranging from a few micrometres to a maximum of approximately 15 μm. Small prismatic shapes are also observed, which are likely fragments of

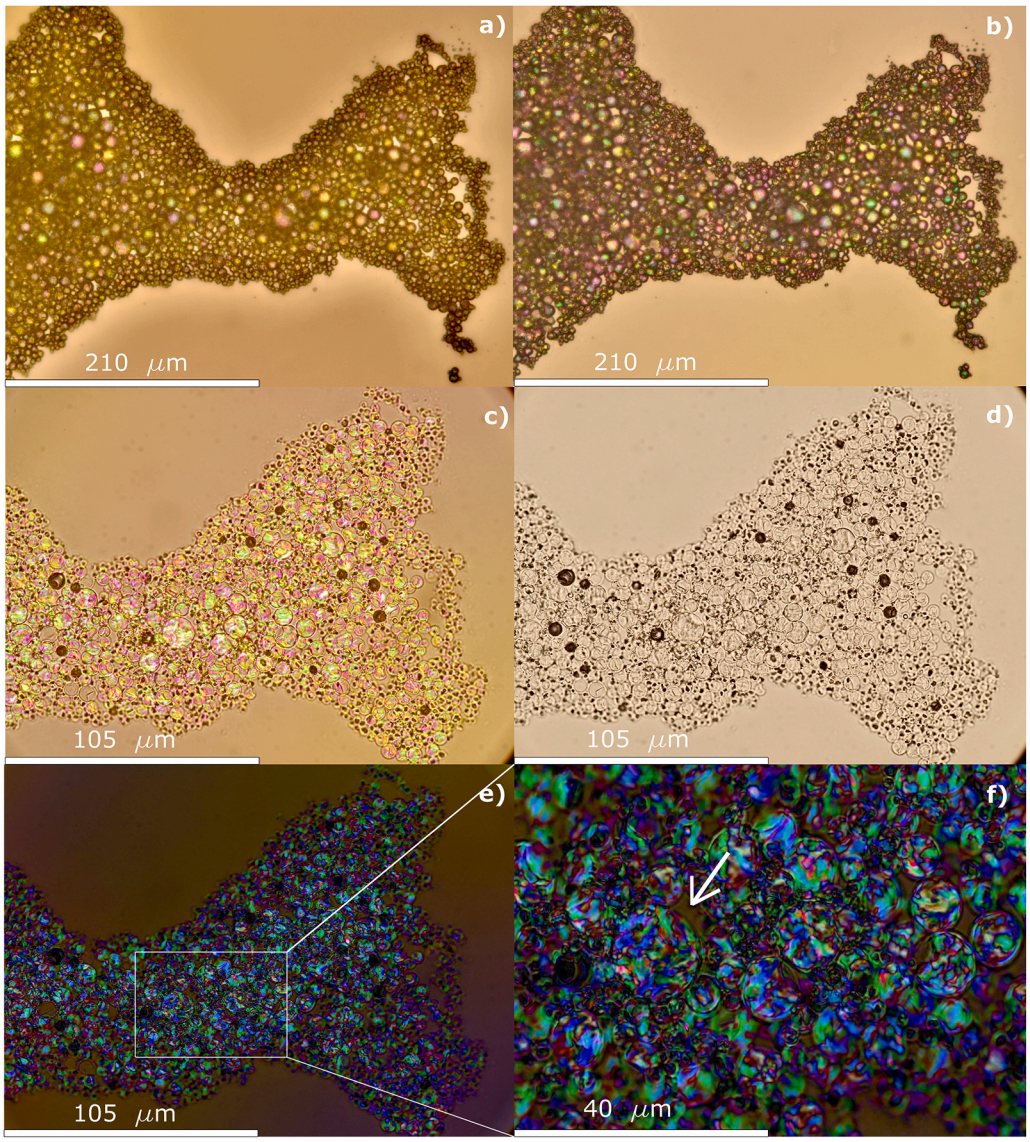

Fig. 5. Photomicrographs taken before and after the heat treatment of dry slurry mPCMs: a) Pre-heating sample photo at 50x; polychromatic polarization (PPM) Different colours within spheres indicate crystals with different crystallographic orientation; b) Post-heating sample photo at 50x; PPM; c) Post-heating micrograph with oil immersion, 100x magnification. Within larger spheres polycrystalline aggregates of crystalline wax can be observed PPM; d) Idem, under plane-polarized light. Arrows point to re-entrants on the surface of spheres; e) Post-heating sample under differential PPM imaging with oil immersion 100x; f) Detail of (e), showing the nanocrystalline aggregates of hundreds of paraffin wax crystals within larger spheres (arrows).

paraffin wax resulting from the rupture of some capsules, (Fig. 7c). This indicates that a limited fraction of microcapsules may already be damaged prior to thermal cycling. Observing the comparison with the microcapsules treated via DSC, it is evident that the spherical structure is preserved but appears more damaged as highlighted in Fig. 7d, with the presence of indentations and recesses in the spheres, similar to those observed by optical microscopy, likely linked to volume variations resulting from heating and cooling cycles [78,79].

The mortar sample containing mPCM (mix 14.6% mPCM+S) shows a high concentration of prismatic shapes too, that can be observed on the surface of the microcapsules in Fig. 7f, likely resulting from the further rupture and damage of the microcapsules following the thermal cycles performed. As depicted in Fig. 7e, here the mortar structure is clearly observed, particularly the tabular forms of cement hydration products such as portlandite [80]. In contrast, the spherical shapes of the microcapsules are rarely found, embedded within the cement matrix, with those present measuring at most a few micrometres. Additionally, some structures exhibiting anomalous curvatures are observed, which cannot be associated with any of the previously noted formations. These are likely remnants of broken microcapsules resulting from the thermal cycles endured.

3.4. Thermal evaluation of cement mortar with and without mPCMs

3.4.1. Differential Scanning calorimetry (DSC) analysis of cement mortar mixes

According to Differential Scanning calorimetry tests, the phase change temperature (melting point) and Latent Heat (ΔH) of the mortar mixes with mPCMs and single mPCM were measured. Initially, individual heating and cooling cycles were performed at a constant rate of 5 °C/min and a temperature range from 35 °C to 95 °C. Samples of wet and dry mPCM, ref. mix 0% mPCM+S and mortar with mPCMs were treated. As depicted in Fig. 8a, it is immediately visible that this type of mPCM has three main melting peaks (between 60 °C and 75 °C) and two solidification peaks (at 64 °C and 46.5 °C). The estimated latent heats for dry mPCMs are 196 J/g and for wet mPCMs around 65 J/g. Similar

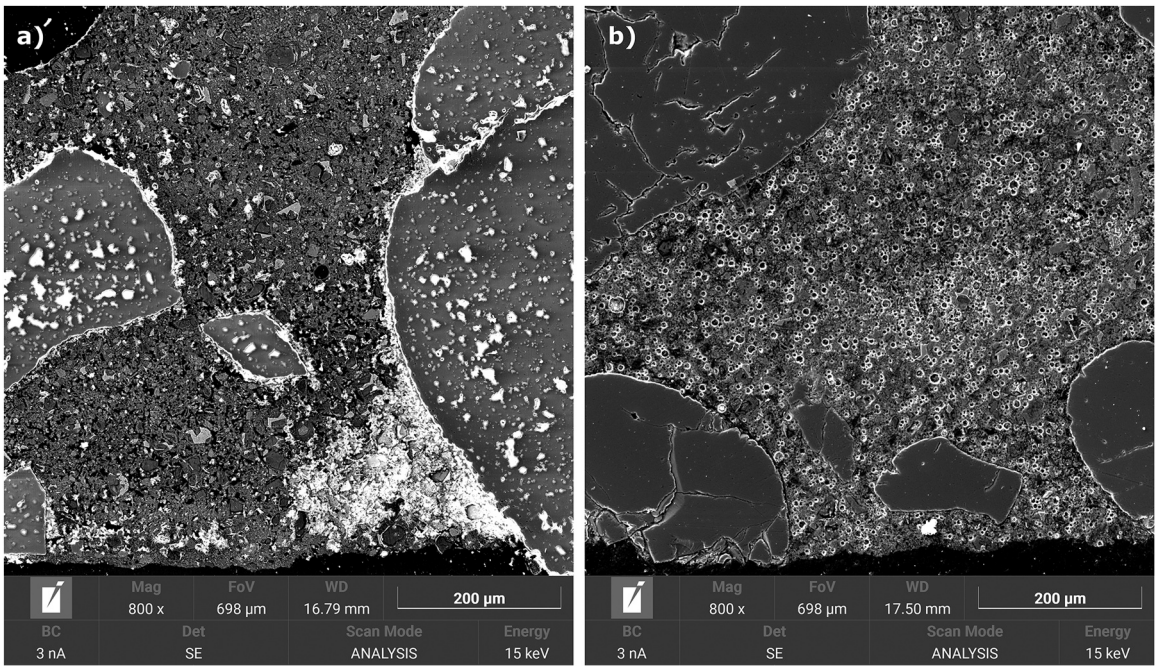

Fig. 6. SEM images of ref. mix 0% mPCM + S and of mix 14,6% mPCM + S, post-compressive strength tests, embedded in resin tablets. These images were taken with an energy of 15 keV. a) Top of the ref. mix 0% mPCM + S, carried out with secondary electrons (SE); b) Top of the mix 14,6% mPCM + S, carried out with secondary electrons (SE). The presence of microcapsules can only be seen in the right sample (mix 14,6% mPCM + S) with a homogeneous distribution.

multi-peak behavior has been reported for commercial paraffin-based PCMs composed of various constituents, where distinct melting and freezing peaks were attributed to incongruent phase change processes of the different components, as demonstrated by dynamic DSC analyses [81].

For wet mPCMs, peaks are observed at slightly different temperatures than for dry mPCMs, especially the minor peak, which appears at lower temperatures, both in melting and in solidification phases (Fig. 8b). This shift can be attributed to the interaction between the encapsulated PCM and the surrounding aqueous medium, which affects heat transfer conditions and phase transition kinetics. Furthermore, from the ratios of the measured latent heats, it is possible to estimate a weight percentage of about 36% mPCM in the slurry. Ref. Mix 0% mPCM+S, without mPCM, was also tested, which obviously shows no peaks related to phase transitions.

Subsequently, as mentioned before, the mortar specimens with the various concentrations of mPCMs slurry (8.0%, 10.6%, 11.9% and 14.6%) were first analysed with individual heating and cooling cycles. Sampling was carried out in the top, middle and bottom of the sample, once again, to see a possible change in the distribution of mPCMs within the cement matrix. These samples also show the multiple peaks associated with the melting and solidification of mPCMs, but they do not exactly match those observed in dry mPCMs. Similar phase change point shifts have been attributed in the literature to interfacial interactions between PCM molecules and the host material, where physical confinement and surface effects influence the phase transition temperature of the embedded PCM compared to its isolated form [82]. Based on the DSC analysis curve, the melting temperatures of the mortars containing mPCMs are slightly lower than mPCMs, this could indicate some interaction between the cement mortar and the microcapsules. DSC profiles also, measured for the same samples, but at various locations, show latent heats of fairly comparable amounts. This indicates a relatively homogeneous distribution of mPCMs within the matrix, in agreement with the micro-Raman and SEM observations.

Finally, 30 heating and cooling cycles were performed between 30 °C and 95 °C at 5 °C/min. The samples that were thermally cycled were the dry and wet mPCMs, the ref. Mix 0% mPCM+S (with sealed and perforated capsule) and mix 14.6% mPCM+S (in this case, the portion to be treated was taken from the central part of the specimens). Cycles carried out on dry microencapsulated PCM show variability in behaviour during the first 2–3 cycles, and then show stabilisation, as can be observed in Fig. 8c. This initial variability is commonly associated with the thermal conditioning of PCM systems and with the progressive stabilization of phase transition mechanisms during early cycles. The steady state behaviour shows a double melting peak, with a minor one at around 67 °C and a major one at 75 °C, with a total latent heat of around 180 J/g (Fig. 8d). The persistence of well-defined melting peaks after repeated cycling confirms that the PCM retains its phase change functionality over the investigated thermal cycles. The peaks shown in the figures represent melting if negative, solidification if positive.

Ref. mix 0% mPCM+S, not containing mPCM, as mentioned before, does not show any peaks related to phase transitions (Fig. 9). The peaks typically associated with mPCMs are absent. All samples containing mPCMs show a certain uniformity of behaviour and the measured latent heats show a trend that follows the relative concentrations of mPCM used in the preparation. All specimens also show a gradual drift in the position and width of the peaks, even if not dramatically, faster in the first cycles and tending to stabilise in about ten cycles. Such peak drift is indicative of minor thermal or structural rearrangements within the PCM during repeated cycling, as reported in previous studies on thermally cycled PCMs [83]. In addition, the amount of latent heat available tends to decrease slightly with cycling, ranging from about 5–20% depending on the samples, with higher losses for specimens containing less mPCM. This behaviour suggests that mortars with lower PCM content may be more sensitive to relative losses of latent heat, while higher mPCM concentrations provide a more stable thermal response over time. As an example, DSC graphs of the sample Mix 14.6% mPCM+S are shown in Fig. 10. The results show a certain uniformity in peaks positions, in the behaviour and in values of latent heats, calculated in relation to the concentration of mPCM added to the cement mortar. Again, as the number of cycles increases, there is a shift from three to two peaks in the heating phase.

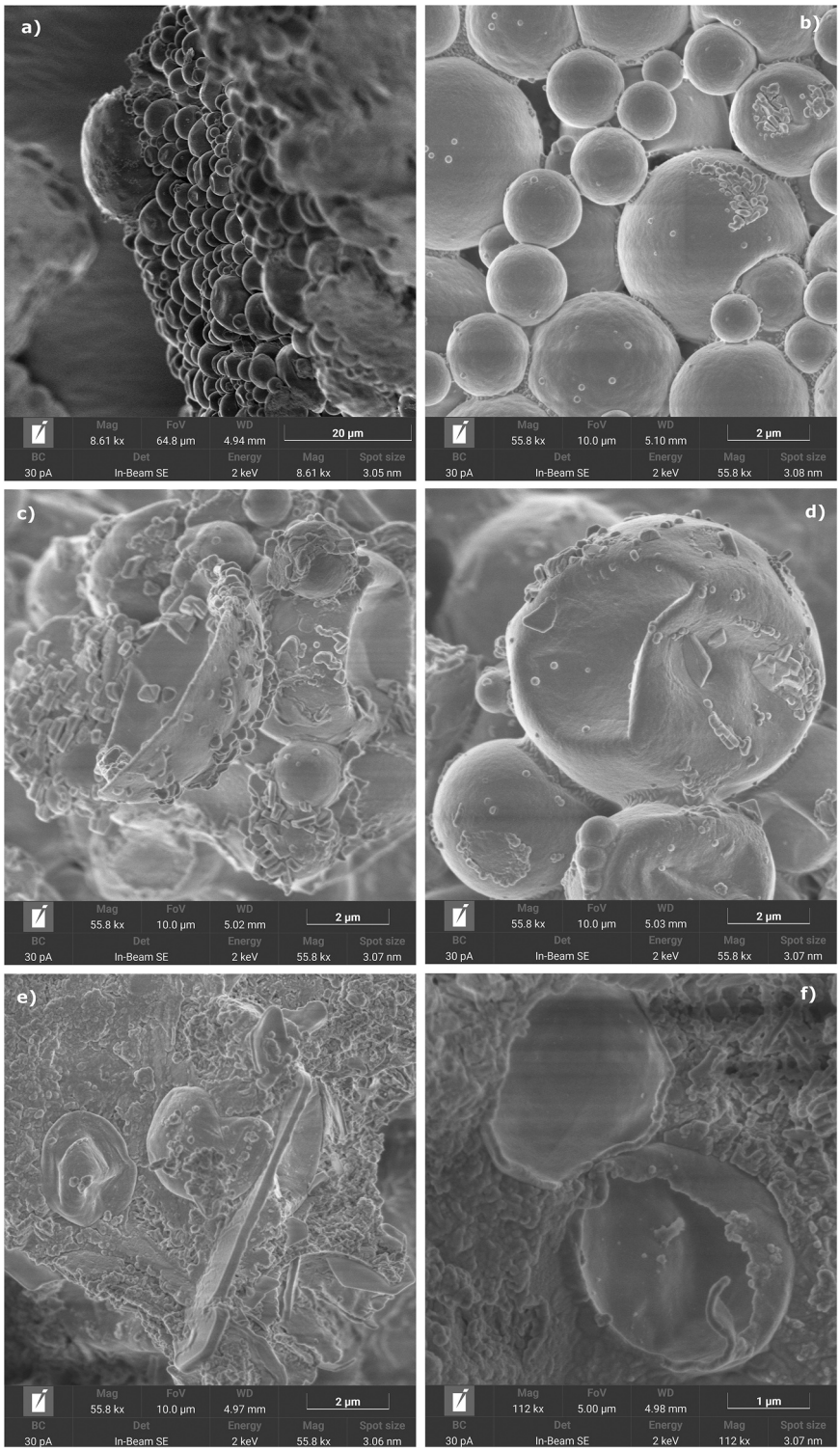

Fig. 7. SEM images of: a,b) Dry mPCM slurry (before heat-treatment); c,d) Dry mPCMs slurry (after heat-treatment); e,f) Sample mix 11,9% mPCM + S (after heat-treatment). All samples were covered with carbon and chrome coating and all images were taken using In-Beam SE with an energy of 2 keV.

3.4.2. Thermal conductivity of cement mortar mixes

Thermal conductivity (k) is the property of a material that determines its ability to transfer heat. It quantifies how efficiently heat moves through a substance due to a temperature gradient. Thermal conductivity of specimens was measured after 28 days of curing and results, for the measurements of ref. mix 0% mPCM + S and samples with mPCMs, are shown in Table 7. Both Thermal conductivity (k) and Thermal Diffusivity (α) measured values acquired by TCS at room temperature (20°C) are reported in Table 7. Please note that the measurements on the mPCM slurry were performed only by using MTPS, so that the thermal diffusivity was not acquired.

According to the results of Thermal Conductivity Scanner (TCS) the heat transfer rates of the mortar containing mPCMs were observed to be lower in comparison to those without mPCMs (i.e., 0% mPCMs). The thermal conductivity measurement indicates that the average k value of the mortar with mPCMs is lower than that obtained from the ref. mix 0%

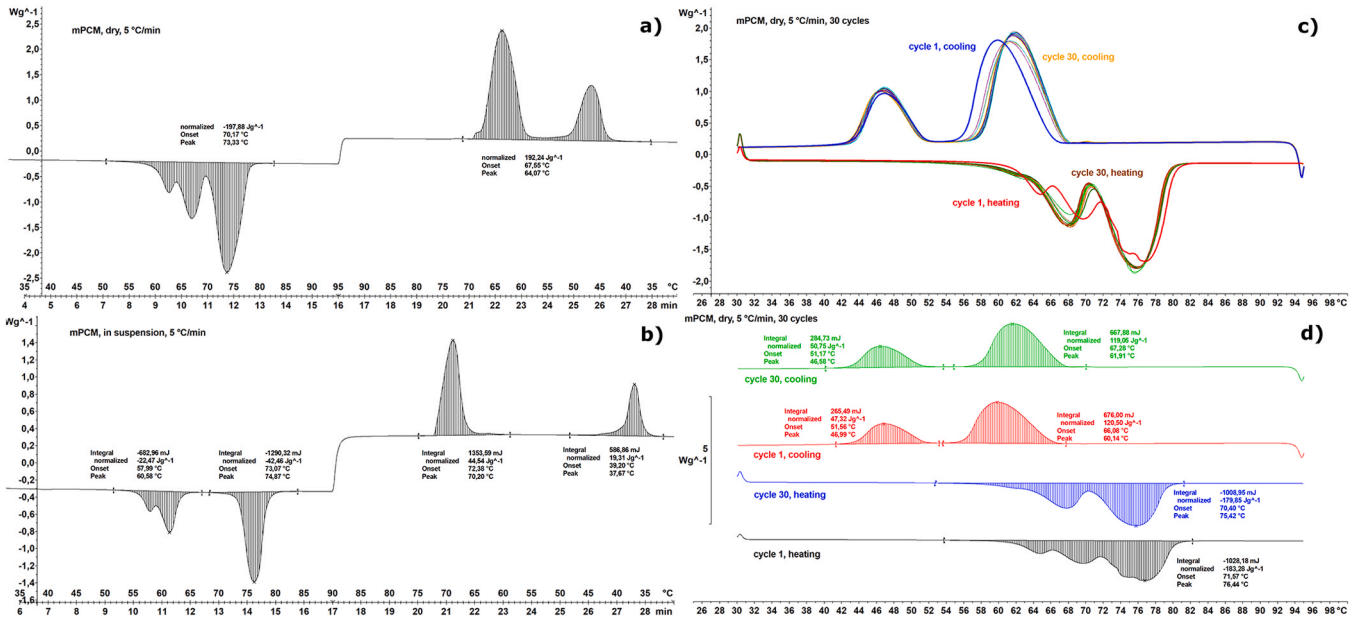

Fig. 8. DSC results for mPCM slurry. a) Single heating and cooling cycle with a constant rate of 5 °C/min from 35 °C to 95 °C for dry mPCM slurry; b) Single heating and cooling cycle with a constant rate of 5 °C/min from 35 °C to 95 °C for mPCM slurry in suspension; c) 30 heating and cooling cycles performed between 30 °C and 95 °C at 5 °C/min for dry mPCM slurry; d) Detail of the first and last cycle for dry mPCM slurry, showing the merging of heating peaks from three to two as the cycles progress.

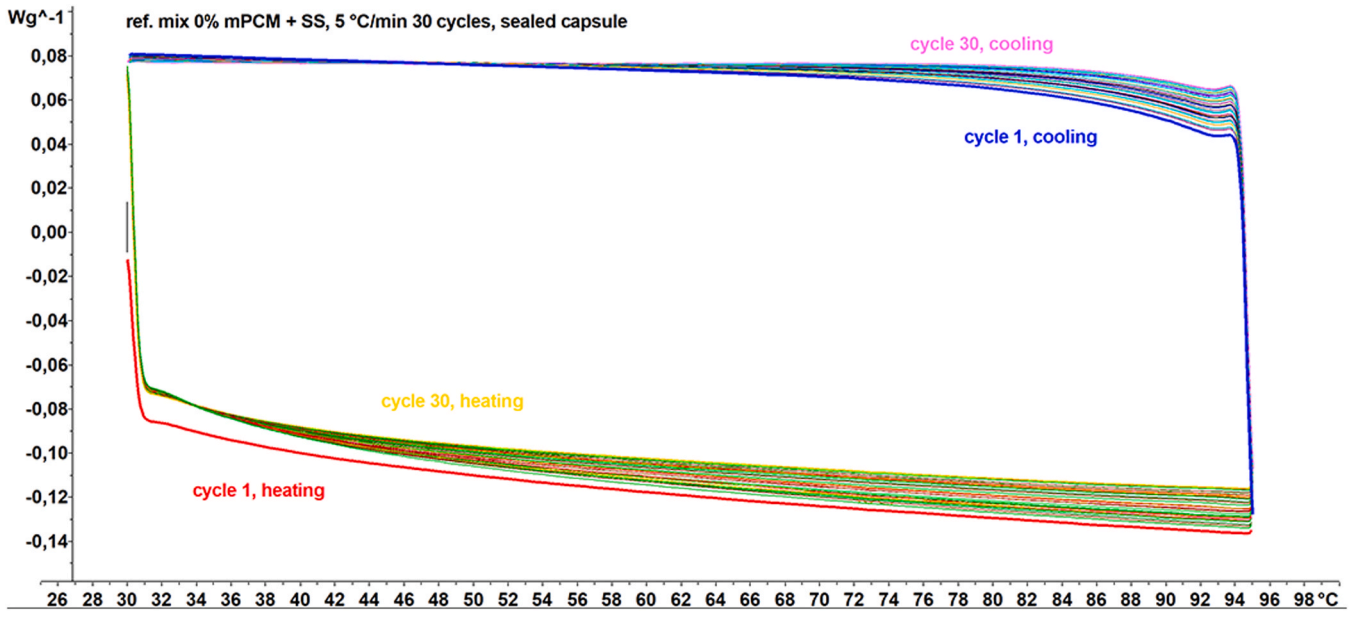

Fig. 9. DSC results for the reference mix 0% mPCM + S over 30 cycles, performed at a constant heating and cooling rate of 5 °C/min, within a temperature range of 30 °C to 95 °C.

mPCM + S sample (i.e., without mPCMs) of 2.23 W/(m·K) at room temperature. This *k* decreased from 1.93 W/(m·K) to 1.48 W/(m·K) (at room temperature) with the addition of mPCMs from 8.0% to 14.6% of concentration, with a maximum reduction in thermal conductivity of approximately 33.5% for the sample containing the highest concentration of mPCMs. Thermal conductivity of the mortar with mPCMs decreased further with the increase in the mPCMs content ratio in the mortar. This reduction can be attributed to the combined effect of the low intrinsic thermal conductivity of the PCM phase and the increased porosity introduced by the slurry-based incorporation of mPCMs, which enhances the presence of air-filled voids acting as thermal insulation. It was also observed that the *k* changes depending on whether the measurement was taken in the bottom, side or top of the sample. This spatial variability is attributed to local differences in pore structure and moisture content within the mortar, since thermal conductivity in cementitious materials is strongly governed by air-void distribution and degree of saturation [84].

Thermal Diffusivity (α) is a material property that describes how quickly heat spreads through a substance when exposed to a temperature gradient. It quantifies the rate at which heat diffuses within a material, considering both its thermal conductivity and its ability to store heat (specific heat capacity and density). With increasing mPCM content, thermal conductivity (k) decreases, while thermal diffusivity (α) shows a more moderate reduction. The measured thermal diffusivity

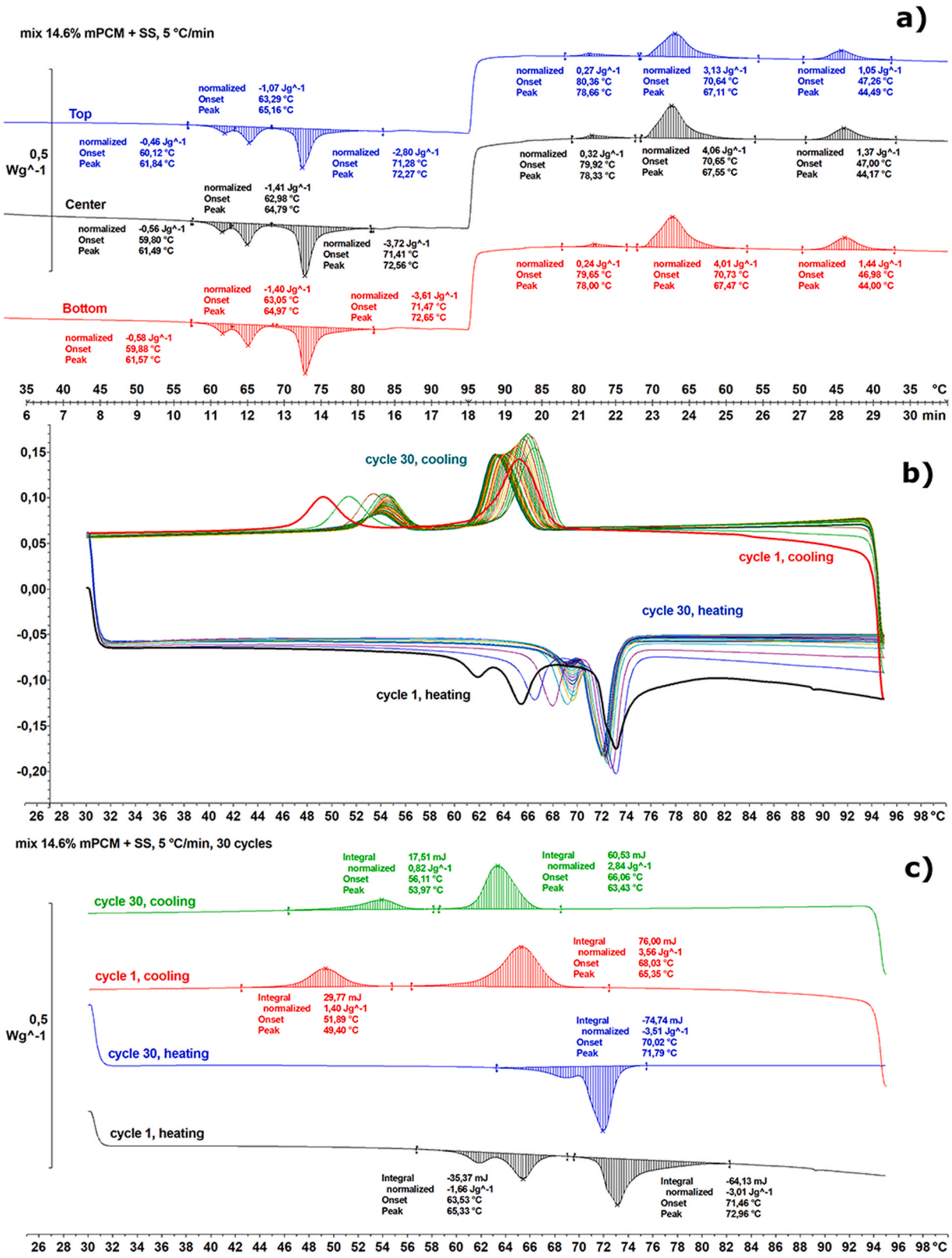

Fig. 10. DSC results for mix 14,6% mPCM + S. a) Comparison of results from sampling at the top, middle, and bottom of the sample, obtained through individual heating and cooling cycles conducted at a rate of 5 °C/min, ranging from 35 °C to 95 °C; b) 30 heating and cooling cycles performed between 30 °C and 95 °C at 5 °C/min; c) Detail of the first and last cycle.

Table 7
Thermal conductivity and thermal diffusivity values for mixed mortar samples and mPCMs slurry measured by TCS at 20 °C. Thermal conductivity and thermal effusivity values of mixed mortar samples and mPCMs slurry measured by MTPS at 80 °C.

		at T = 20 °C		at T = 80 °C	
Mix ID	% PCM	Thermal conductivity [W/(m*K)]	Diffusivity [m^2/s]	Thermal conductivity [W/(m*K)]	Effusivity ($Ws^{1/2}/m^2K$) - 80 °C
Ref. Mix 0% mPCM+S	0.00	2.23	1.20E-06	2.64	2 249.00
Mix 8.0% mPCM+S	8.00	1.93	1.073E-06	2.41	2 131.70
Mix 10.6% mPCM+S	10.60	1.75	9.67E-07	2.37	2 112.00
Mix 11.9% mPCM+S	11.90	1.72	9.88E-07	2.18	2 012.10
Mix 14.6% mPCM+S	14.60	1.48	9.58E-07	2.01	1 923.30
mPCM slurry	100.00	0.46	/	0.44	1 267.10

values (Table 7) demonstrate that despite a 33.5% reduction in thermal conductivity at maximum mPCM loading, thermal diffusivity decreases by only 20%.

Thermal Diffusivity (α) [m^2/s] and Thermal conductivity (k) are strictly correlated as here expressed:

$$\alpha = \frac{k}{\rho c_p} \tag{2}$$

where k is the thermal conductivity [W/(m·K)], ρ is the density [kg/m^3] and c_p is the specific heat capacity [J/(kg·K)]. This relationship indicates that the volumetric heat capacity (ρ·cp) also decreases upon mPCM addition, although to a lesser extent than thermal conductivity. The observed disparity between the reduction rates provides valuable insight into the microstructural changes induced by mPCM incorporation. The pronounced decrease in k (up to 33.5%) compared to the moderate reduction in α suggests that the concurrent decrease in bulk density partially counterbalances the effect of reduced thermal conductivity. The thermal mass per unit volume decreases proportionally with thermal conductivity, consistent with the replacement of denser cementitious matrix with lighter mPCM-containing regions and air voids.

From a thermal performance perspective, this behaviour has significant implications: while the reduced thermal conductivity enhances the insulation properties of the material, the moderately decreased thermal diffusivity indicates that the material retains a reasonable capacity for thermal energy propagation. This balance is particularly advantageous for thermal energy storage applications, where both insulation (low k) and heat distribution (adequate α) are desirable.

Subsequently, the samples were measured with the Modified Transient Plane Source method (MTPS) technique from the Trident instrument (C-Therm). Thermal conductivity of all samples and mPCM slurry were measured at a temperature of 80 °C with this instrument, being the only instrument that can enter inside the oven. The results are reported in Table 7; thermal conductivity values measured by C-Term at 80°C appear slightly higher than that measured at 20°C by TCS, but the general trend indicate the decrease in k as the concentration of mPCM in the cement paste increases. The higher values measured by MTPS compared to TCS are attributed to methodological differences (sensor geometry and contact conditions), while the consistent trend confirms the robustness of the observed effect of mPCM addition on k.

With this instrument, it was also possible to measure Thermal Effusivity (e) [$Ws^{1/2}/(m^2·K)$], also reported in Table 7:

$$e = \sqrt{k\rho c_p} \tag{3}$$

Thermal Effusivity is a material property that describes its ability to exchange heat with its surroundings. It represents the absorbing and releasing thermal energy capacity of a material, when it is put in contact with another surface. Accordingly, the decrease in e with increasing mPCM content reflects a reduced ability of the composite to exchange heat rapidly with the environment, which is consistent with the combined reduction in k and ρ. Thanks to a container, suitable for measuring liquid and powder samples, it was also possible to measure k and e of the mPCM slurry, at average room temperature (of around 20 °C) and inside the owen at 80 °C, resulting respectively [$k = 0.46$ W/(m·K) and $e = 1319{,}20$ $Ws^{1/2}/(m^2·K)$ at 20 °C] and [$k = 0.44$ W/(m·K) and $e = 1267.1$ $Ws^{1/2}/(m^2·K)$ at 80 °C.

It can be observed that all these k values are higher than the data taken at room temperature, but still respect the decreasing trend of k as the concentration of mPCM in the cement mortar mix increases. The only exception can be made for measurements on single mPCMs, which at 80 °C show lower k and e values than that of 20 °C (Fig. 11). This difference can be attributed to the temperature-dependent thermophysical behavior of paraffin-based PCMs, especially near or above their phase transition range. [85] reported that changes in phase state and density with temperature significantly affect the thermal conductivity and related transport properties of paraffin PCMs.

4. Conclusions

This study investigated the effect of incorporating microencapsulated phase change materials (mPCMs) slurry into mortars through a complete thermo-mechanical and microstructural characterization of mixtures of mPCMs and mortars at different percentages. We investigated the bulk density, compressive and flexural strength, microstructure, latent heat, and thermal conductivity of these mixed mortars and assessed their suitability for thermal energy storage (TES) applications.

The main conclusions can be summarised as follows:

1. The incorporation of mPCM slurry resulted in a reduction of bulk density of up to 11%. This behaviour is primarily attributed to the lower intrinsic density of the microcapsules and to the additional water introduced with the slurry, but is also influenced by increased porosity and entrapped air, as evidenced by SEM observations;
2. Compressive strength decreased by 30 – 48% with increasing mPCM slurry content, while flexural strength showed a similar declining trend. Beyond water content effects, this mechanical deterioration is associated with the presence of mPCMs as mechanically weaker inclusions and increased air voids, which collectively reduce the effective load capacity of the hardened mortar;
3. SEM and micro-Raman spectroscopy analyses confirmed a homogeneous distribution of mPCMs within the cement matrix, with no significant segregation effects;
4. Optical microscopy observations showed that microcapsules mainly maintain their structural integrity after 30 thermal cycles, with no significant damage observed, demonstrating their durability across multiple thermal cycles;
5. DSC analysis showed that material behaviour stabilizes after the first few iterations, with latent heat losses ranging from 5 to 20%, after 30 thermal cycles. The latent heat storage capacity of the mortars increased proportionally with mPCM content, with a total gain in heat capacity of about 5 kJ/kg, confirming the effectiveness of mPCM incorporation for enhancing thermal energy storage potential.
6. Thermal conductivity decreased by up to 33.5% with increasing mPCM content at both ambient and elevated temperatures, while

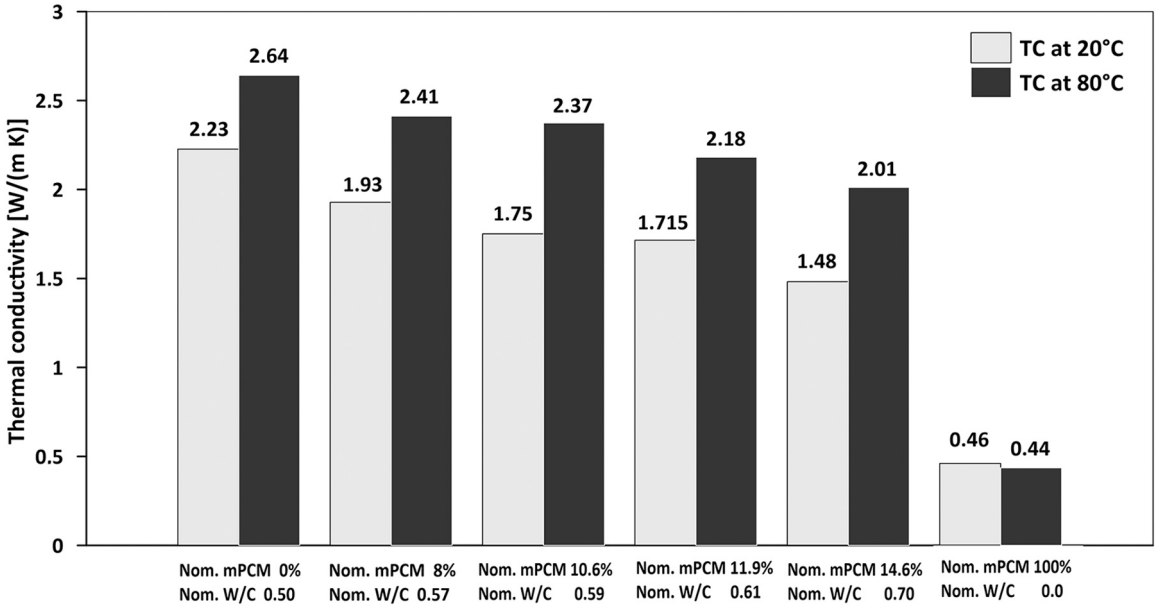

Fig. 11. Comparison of Thermal conductivity of mixed mortar samples and mPCMs slurry at 20 °C (TCS) and 80 °C (MTPS).

thermal effusivity followed the same trend, indicating reduced heat exchange capacity.

The findings confirm the feasibility of integrating mPCM slurry with a phase transition temperature around 70 °C into cementitious mortars for medium temperature thermal energy storage applications, demonstrating their potential, despite certain challenges associated with mix preparation. The widely available and cost-effective cement mortar enhances the confinement of microencapsulated PCMs, preventing their dispersion within the mixture. Additionally, its quartz-rich composition contributes to improve thermal conductivity as it emerges by observing thermal conductivity ranges of the mixes compared to the single mPCM slurry.

Unfortunately, the high cost and limited commercial availability of mPCM slurries, particularly within the desired temperature range (~70°C), can present challenges for large-scale implementation. Moreover, the poor workability of mPCM-enhanced mortars necessitates optimization of mix formulation via superplasticisers to achieve desirable handling properties. The presence of formaldehyde in the microcapsule shell poses potential health risks, particularly at elevated temperatures (~100°C), where volatile emissions may occur. While mPCMs improve TES efficiency, given the obtained increase in latent heat, their incorporation results in lower thermal conductivity compared to ref. mix 0% mPCM+S. This reduced conductivity slows down the thermal charge and discharge rate, potentially affecting the dynamic performance of the storage system in applications requiring rapid thermal reaction. In addition, decline in compressive and flexural strength was observed in samples with increasing mPCM concentrations, highlighting the need for strategies to mitigate mechanical deterioration, in case TES solutions are intended for integration into building foundations and other energy geostructures.

This study was also subjected to several limitations. The investigation was conducted on mortars rather than concrete, using a single type of paraffin wax mPCM slurry. Mixed mortars required adjustments to water content to maintain workability, and thermal durability was assessed over a limited number of cycles (30). Long-term durability, ageing effects and large-scale structural behaviour were not addressed and should be considered in future research. Although the identified limitations, the results highlight several positive features of the adopted mPCM slurry system. The microcapsules exhibited good structural and thermal stability, retaining a substantial fraction of their latent heat capacity after repeated heating–cooling cycles and showing no significant segregation within the cement matrix. Their homogeneous dispersion, combined with stable phase-change behaviour, facilitates a measurable increase in the overall energy storage potential of the mortar. Although the incorporation of mPCMs reduces thermal conductivity, the added latent heat capacity enhances the effective thermal inertia of the composite and contributes to a more gradual and delayed thermal response during charging and discharging processes.

These findings corroborate that mPCM slurry with a melting range around 70 °C can effectively improve medium-temperature TES performance when embedded in cement-based materials. The widely available and cost-effective cement mortar enhances the confinement of microencapsulated PCMs, preventing their dispersion within the mixture. Furthermore, its quartz-rich composition contributes to improved thermal conductivity, as evidenced by the thermal conductivity ranges of the mixes compared to the single mPCM slurry.

Considering that the primary objectives of this study were to identify optimal trade-offs between thermal conductivity and thermal storage capacity, as well as to evaluate the operational behavior and structural stability of phase change materials under repeated phase transition cycles, future experimental studies could improve upon the results obtained here by enhancing knowledge of the workability and stability of mixed mPCM slurry mortars.

Other important future developments of this study could focus on the integration of mPCM-doped mortar into TABS, analyzing its boosting effects on thermal energy storage and peak load shifting while maintaining sufficient mechanical strength through PCM microencapsulation, taking into account the importance of careful mix design required to balance the increased thermal inertia with potential impacts on structural density. This evaluation should encompass the overall thermal energy storage efficiency, which is dependent not only on the properties of the storage material itself but also on heat exchanger configuration, storage geometry, and operational strategies. Such comprehensive analysis should be conducted at the system level to provide a holistic understanding of mPCM performance in practical applications also considering long-term durability and lifecycle performance, in order to improve the thermal storage solutions.

Funding sources

This work was supported by the MUR Italian PNRR project NEST -

NETWORK 4 ENERGY SUSTAINABLE TRANSITION (PE2 Spoke 6) and by the SINERGHY project, PR FESR 2021, Veneto Region RIR funds. The authors are also grateful to the FOE FUTURAW Project that partially supported the research.

CRediT authorship contribution statement

Enrico Garbin: Writing – review & editing, Validation. **Filippo Agresti:** Writing – review & editing, Investigation. **Bernardo Cesare:** Writing – review & editing, Investigation. **Simona Barison:** Writing – review & editing, Investigation. **Maria Chiara Dalconi:** Writing – review & editing, Supervision, Investigation, Conceptualization. **Sara Franzè:** Writing – review & editing, Writing – original draft, Visualization, Investigation, Formal analysis, Data curation. **Antonio Galgaro:** Writing – review & editing, Supervision, Funding acquisition, Conceptualization. **Giorgia Dalla Santa:** Writing – review & editing, Supervision, Conceptualization.

Declaration of Competing Interest

The authors declare that they have no known competing financial interests or personal relationships that could have appeared to influence the work reported in this paper.

Data availability

Data will be made available on request.

References

[1] J. Twidell, T. Weir, Renew. energy resources, Taylor & Francis Group, Routledge, 2015, https://doi.org/10.4324/9781315766416.
[2] M. Iten, S. Liu, A. Shukla, A review on the air-PCM-TES application for free cooling and heating in the buildings, Renew. Sustain. Energy Rev. 61 (2016) 175–186, https://doi.org/10.1016/j.rser.2016.03.007.
[3] V. Burton, Renew. energy: sources, applications and emerging technologies, Nova Science Publishers, 2016.
[4] T. Brief, IEA-ETSAP and IRENA © Technology Brief E17-Thermal Energy Storage Energy Technology Systems Analysis Programme, 2013. ⟨www.etsap.org-www.irena.org⟩.
[5] I. Sarbu, C. Sebarchievici, A comprehensive review of thermal energy storage, Sustainability 10 (2018), https://doi.org/10.3390/su10010191.
[6] I. Dincer, S. Dost, X. Li, Performance analyses of sensible heat storage systems for thermal applications, Int. J. Energy Res. 21 (1997) 1157–1171, https://doi.org/10.1002/(SICI)1099-114X(19971010)21:12<1157::AID-ER317>3.0.CO;2-N.
[7] R. Mabrouk, H. Naji, A.C. Benim, H. Dhahri, A state of the art review on sensible and latent heat thermal energy storage processes in porous media: mesoscopic simulation, Appl. Sci. 12 (2022) 6995, https://doi.org/10.3390/app12146995.
[8] K. Lovegrove, J. Pye, Fundamental principles of concentrating solar power (CSP) systems, in: Concentrating Solar Power Technology, Elsevier, 2012, pp. 16–67, https://doi.org/10.1533/9780857096173.1.16.
[9] T. Nomura, N. Okinaka, T. Akiyama, Technology of latent heat storage for high temperature application: a review, ISIJ Int. 50 (2010) 1229–1239, https://doi.org/10.2355/isijinternational.50.1229.
[10] S. Raoux, Phase change materials, Annu. Rev. Mater. Res. 39 (2009) 25–48, https://doi.org/10.1146/annurev-matsci-082908-145405.
[11] R. Salgado-Pizarro, A. Calderón, A. Svobodova-Sedlackova, A.I. Fernández, C. Barreneche, The relevance of thermochemical energy storage in the last two decades: the analysis of research evolution, J. Energy Storage 51 (2022) 104377, https://doi.org/10.1016/j.est.2022.104377.
[12] S.J. Osibodu, A.M. Adeyinka, O.V. Mbelu, Phase change material integration in concrete for thermal energy storage: techniques and applications in sustainable building, Sustain. Energy Res. 11 (2024) 45, https://doi.org/10.1186/s40807-024-00138-8).
[13] Y. Qu, Q. Li, L. Cai, M. Pan, P. Ghosh, K. Du, M. Qiu, Thermal camouflage based on the phase-changing material GST, Light Sci. Appl. 7 (2018), https://doi.org/10.1038/s41377-018-0038-5.
[14] A. Mishra, A. Shukla, A. Sharma, Latent heat storage through phase change materials, Resonance 20 (6) (2015) 532–541, https://doi.org/10.1007/s12045-015-0212-5.
[15] R.E. Simpson, P. Fons, A.V. Kolobov, T. Fukaya, M. Krbal, T. Yagi, J. Tominaga, Interfacial phase-change memory, Nat. Nanotechnol. 6 (2011) 501–505, https://doi.org/10.1038/nnano.2011.96.
[16] D. Lee, S.-G. Lee, S. Kim, A.M. Asce, Composite Phase-Change Material Mold for Cost-Effective Production of Free-Form Concrete Panels, (2017). https://doi.org/10.1061/(ASCE).
[17] A. Sharma, V.V. Tyagi, C.R. Chen, D. Buddhi, Review on thermal energy storage with phase change materials and applications, Renew. Sustain. Energy Rev. 13 (2009) 318–345, https://doi.org/10.1016/j.rser.2007.10.005.
[18] L.M. Bal, S. Satya, S.N. Naik, Solar dryer with thermal energy storage systems for drying agricultural food products: A review, Renew. and, Sustain. Energy Rev. 14 (2010) 2298–2314, https://doi.org/10.1016/j.rser.2010.04.014.
[19] B. Zalba, J.M. Marín, L.F. Cabeza, H. Mehling, Review on thermal energy storage with phase change: materials, heat transfer analysis and applications, Appl. Therm. Eng. 23 (3) (2003) 251–283, https://doi.org/10.1016/S1359-4311(02)00192-8.
[20] N. Kumar, D. Banerjee, Phase Change Materials. Handb. of Therm. Science and Engineering, Springer International Publishing, Cham, 2018, pp. 2213–2275, https://doi.org/10.1007/978-3-319-26695-4_53.
[21] R.K. Sharma, P. Ganesan, V.V. Tyagi, H.S.C. Metselaar, S.C. Sandaran, Developments in organic solid-liquid phase change materials and their applications in thermal energy storage, Energy Convers. Manag 95 (2015) 193–228, https://doi.org/10.1016/j.enconman.2015.01.084.
[22] W. Su, J. Darkwa, G. Kokogiannakis, Review of solid-liquid phase change materials and their encapsulation technologies, Renew. Sustain. Energy Rev. 48 (2015) 373–391, https://doi.org/10.1016/j.rser.2015.04.044.
[23] R. Bharathiraja, T. Ramkumar, M. Selvakumar, Studies on the thermal characteristics of nano-enhanced paraffin wax phase change material (PCM) for thermal storage applications, J. Energy Storage 73 (2023) 109216, https://doi.org/10.1016/j.est.2023.109216.
[24] I. Sarbu, C. Sebarchievici, A comprehensive review of thermal energy storage, Sustain. (Switz.) 10 (2018), https://doi.org/10.3390/su10010191.
[25] W.-Y. Wu, M. Gao, R. Yeo Jueyuan, M. Lin, S. Wang, W. Thitsartarn, X. Zhang, D. Kai, P. Wang, Z. Qu, J. Xu, X. Jun Loh, Q. Zhu, Plant oil-based phase change materials for sustainable thermal energy storage: A review, Fuel 378 (2024) 132940, https://doi.org/10.1016/j.fuel.2024.132940.
[26] S. Sundararajan, A.B. Samui, P.S. Kulkarni, Versatility of polyethylene glycol (PEG) in designing solid–solid phase change materials (PCMs) for thermal management and their application to innovative technologies, J. Mater. Chem. A 5 (2017) 18379–18396, https://doi.org/10.1039/C7TA04968D.
[27] G.S. Parks, T.J. West, B.F. Naylor, P.S. Fujii, L.A. McClaine, Thermal data on organic compounds xxiii modern combustion data for fourteen hydrocarbons and five, J. Am. Chem. Soc. (1946) 2524–2527.
[28] G.S. Parks, J.A. Hatton, Thermal Data on Organic Compounds. XXV. Some Heat Capacity, Entropy and Free Energy Data for Nine Hydrocarbons of High Molecular Weight, J. Am. Chem. Soc. 71 (10) (1949) 3386–3389. ⟨https://pubs.acs.org/sharingguidelines⟩.
[29] A.F. Regin, S.C. Solanki, J.S. Saini, Heat transfer characteristics of thermal energy storage system using PCM capsules: A review, Renew. and, Sustain. Energy Rev. 12 (2008) 2438–2458, https://doi.org/10.1016/j.rser.2007.06.009.
[30] A. Fery, R. Weinkamer, Mechanical properties of micro- and nanocapsules: single-capsule measurements, Polymers 48 (2007) 7221–7235, https://doi.org/10.1016/j.polymer.2007.07.050.
[31] C. Amaral, R. Vicente, P.A.A.P. Marques, A. Barros-Timmons, Phase change materials and carbon nanostructures for thermal energy storage: a literature review, Renew. Sustain. Energy Rev. 79 (2017) 1212–1228, https://doi.org/10.1016/j.rser.2017.05.093.
[32] T. Khadiran, M.Z. Hussein, Z. Zainal, R. Rusli, Encapsulation techniques for organic phase change materials as thermal energy storage medium: a review, Sol. Energy Mater. Sol. Cells 143 (2015) 78–98, https://doi.org/10.1016/j.solmat.2015.06.039.
[33] F.L. Tan, S.F. Hosseinizadeh, J.M. Khodadadi, L. Fan, Experimental and computational study of constrained melting of phase change materials (PCM) inside a spherical capsule, Int. J. Heat. Mass Transf. 52 (2009) 3464–3472, https://doi.org/10.1016/j.ijheatmasstransfer.2009.02.043.
[34] C. Alkan, A. Sari, A. Karaipekli, O. Uzun, Preparation, characterization, and thermal properties of microencapsulated phase change material for thermal energy storage, Sol. Energy Mater. Sol. Cells 93 (2009) 143–147, https://doi.org/10.1016/j.solmat.2008.09.009.
[35] L. Pathak, G.V.N. Trivedi, R. Parameshwaran, S.S. Deshmukh, Microencapsulated phase change materials as slurries for thermal energy storage: a review, Mater. Today. Proc. 44 (2021) 1960–1963, https://doi.org/10.1016/j.matpr.2020.12.101.
[36] P. Zhang, Z.Z. Qiu, M. He, Review on microencapsulated phase change materials (MPCM) slurries: Materials, rheological behavior and applications, in: Adv. Mat. Res., Trans Tech Publications Ltd, 2014, pp. 1109–1112, https://doi.org/10.4028/www.scientific.net/AMR.953-954.1109.
[37] M. Delgado, A. Lázaro, J. Mazo, B. Zalba, Review on phase change material emulsions and microencapsulated phase change material slurries: materials, heat transfer studies and applications, Renew. and, Sustain. Energy Rev. 16 (2012) 253–273, https://doi.org/10.1016/j.rser.2011.07.152.
[38] A. Jamekhorshid, S.M. Sadrameli, M. Farid, A review of microencapsulation methods of phase change materials (PCMs) as a thermal energy storage (TES) medium, SRenew. Sustain. Energy Rev. 31 (2014) 531–542, https://doi.org/10.1016/j.rser.2013.12.033.
[39] G.N. Kumar, B. Al-Aifan, R. Parameshwaran, V.V. Ram, Facile synthesis of microencapsulated 1-dodecanol/melamine-formaldehyde phase change material using in-situ polymerization for thermal energy storage, Colloids Surf. A Physicochem. Eng. Asp. 610 (2021) 125698, https://doi.org/10.1016/j.colsurfa.2020.125698.
[40] D. Salciarini, M. Gerola, S. De Feudis, A. Lupattelli, G. Dalla Santa, G. Capati, M. Rafai, J. Tihana, M. Scerbo, A. Di Donna, E. Ravera, M. Nicolino, A. Insana, H. Mroueh, M. Barla, Database-driven analysis of energy geostructures using a

global dataset: diffusion, efficiency, and environmental performance, Renew. Energy 256 (2026), https://doi.org/10.1016/j.renene.2025.124373.
[41] P. Han, L. Lu, X. Qiu, Y. Tang, J. Wang, Preparation and characterization of macrocapsules containing microencapsulated PCMs (phase change materials) for thermal energy storage, Energy 91 (2015) 531–539, https://doi.org/10.1016/j.energy.2015.08.001.
[42] J. Shi, J. Tan, B. Liu, Y. Liu, H. Xu, Z. Wang, T. Xiong, J. Shi, Thermal and mechanical properties of thermal energy storage lightweight aggregate mortar incorporated with phase change material, J. Energy Storage 32 (2020) 101719, https://doi.org/10.1016/j.est.2020.101719.
[43] B. Šavija, Smart crack control in concrete through use of phase change materials (PCMs): a review, Mater 11 (2018) 654, https://doi.org/10.3390/ma11050654.
[44] H. Cui, W. Liao, X. Mi, T.Y. Lo, D. Chen, Study on functional and mechanical properties of cement mortar with graphite-modified microencapsulated phase-change materials, Energy Build. 105 (2015) 273–284, https://doi.org/10.1016/j.enbuild.2015.07.043.
[45] S. Cunha, J. Aguiar, K. Zalegowski, A. Garbacz, P. Soares, J. Azevedo, V. Ferreira, A. Tadeu, Sustainable mortars with incorporation of microencapsulated phase change materials, Adv. Mat. Res. 1129 (2015) 621–628, https://doi.org/10.4028/www.scientific.net/AMR.1129.621.
[46] A. Ricklefs, A.M. Thiele, G. Falzone, G. Sant, L. Pilon, Thermal conductivity of cementitious composites containing microencapsulated phase change materials, Int. J. Heat. Mass Transf. 104 (2017) 71–82, https://doi.org/10.1016/j.ijheatmasstransfer.2016.08.013.
[47] K. Snehal, B.B. Das, Influence of incorporating phase change materials on cementitious system—a review, Recent Trends Civ. Eng. (2021) 33–63, https://doi.org/10.1007/978-981-15-8293-6_4.
[48] G.W.H. Höhne, W.F. Hemminger, H.-J. Flammersheim, Differential Scanning Calorimetry. Differential Scanning Calorim, Springer Berlin Heidelberg, Berlin, Heidelberg, 2003, pp. 147–244, https://doi.org/10.1007/978-3-662-06710-9.
[49] Popov Y., Lippmann E., Rauen A., TCS-Manual T.C.S. Thermal Conductivity (TC) and Thermal Diffusivity (TD) Scanner, 2020.
[50] N. Wooden, Thermal Conductivity Instrument User Manual, 2023.
[51] P.J.N. Pells, Uniaxial Strength Testing, in: P.J.N. Pells (Ed.), Rock Test. and Site Characterization, Elsevier, 1993, pp. 67–85, https://doi.org/10.1016/B978-0-08-042066-0.50010-0.
[52] J.I. Goldstein, D.E. Newbury, J.R. Michael, N.W.M. Ritchie, J.H.J. Scott, D.C. Joy, Scanning Electron Microscopy and X-Ray Microanalysis (New York), Springer, New York, NY, 2018, https://doi.org/10.1007/978-1-4939-6676-9.
[53] B. Cesare, N. Campomenosi, M. Shribak, Polychromatic polarization: boosting the capabilities of the good old petrographic microscope, Geology 50 (2022) 137–141, https://doi.org/10.1130/G49303.1.
[54] J.R. Ferraro, K. Nakamoto, C.W. Brown, Introductory Raman spectroscopy, Academic Press, 2003.
[55] S. Pilehvar, A.M. Szczotok, M. Carmona, R. Pamies, A.-L. Kjøniksen, The effect of microencapsulated phase change materials on the rheology of geopolymer and Portland cement mortars, J. Am. Ceram. Soc. 103 (2020) 5775–5787, https://doi.org/10.1111/jace.17215.
[56] A. Ismail, J. Wang, B.A. Salami, L.O. Oyedele, G.K. Otukogbe, Microencapsulated phase change materials for enhanced thermal energy storage performance in construction materials: a critical review, Constr. Build. Mater. 401 (2023) 132877, https://doi.org/10.1016/j.conbuildmat.2023.132877.
[57] Y. Ma, L. Jin, S. Wei, L. Wang, X. Zang, J. Zhang, L. Zhang, Multifunctional response mechanisms of PCM-modified mortar: linking particle size distribution to hydration process, thermal conductivity, and strength evolution, Buildings 16 (2026) 803, https://doi.org/10.3390/buildings16040803.
[58] T. Laz, A. Hamami, A. Benjeddou, Impact of microencapsulated phase change materials (PCMs) on the thermal and mechanical performance of cement mortar, Dev. Built Environ. 19 (2024) 100594, https://doi.org/10.1016/j.dibe.2024.100594.
[59] H. Ez-zaki, L. Riva, M. Bellotto, L. Valentini, E. Garbin, C. Punta, G. Artioli, Influence of cellulose nanofibrils on the rheology, microstructure and strength of alkali activated ground granulated blast-furnace slag: a comparison with ordinary Portland cement, Mater. Struct. 54 (2021), https://doi.org/10.1617/s11527-020-01614-5.
[60] British Standards Institution (BSI), BS EN 196-1:2016: Methods of testing cement – Part 1: Determination of strength, BSI, London, 2016.
[61] Y.A. Popov, D.F. Pribnow, J.H. Sass, C.F. Williams, H. Burkhardt, Characterization of rock thermal conductivity by high-resolution optical scanning, Geothermics 28 (2) (1999) 253–276.
[62] N. Wooden, Thermal Conductivity Instrument User Manual, 2023.
[63] H. Abbasi Hattan, M. Madhkhan, A. Marani, Thermal and mechanical properties of building external walls plastered with cement mortar incorporating shape-stabilized phase change materials (SSPCMs), Constr. Build. Mater. 270 (2021), https://doi.org/10.1016/j.conbuildmat.2020.121385.
[64] Z. Zhang, G. Shi, S. Wang, X. Fang, X. Liu, Thermal energy storage cement mortar containing n-octadecane/expanded graphite composite phase change material, Renew. Energy 50 (2013) 670–675, https://doi.org/10.1016/j.renene.2012.08.024.
[65] H. Cui, W. Liao, X. Mi, T.Y. Lo, D. Chen, Study on functional and mechanical properties of cement mortar with graphite-modified microencapsulated phase-change materials, Energy Build. 105 (2015) 273–284, https://doi.org/10.1016/j.enbuild.2015.07.043.
[66] J. Shi, J. Tan, B. Liu, Y. Liu, H. Xu, Z. Wang, T. Xiong, J. Shi, Thermal and mechanical properties of thermal energy storage lightweight aggregate mortar incorporated with phase change material, J. Energy Storage 32 (2020) 101719, https://doi.org/10.1016/j.est.2020.101719.
[67] M. Ren, X. Wen, X. Gao, Y. Liu, Thermal and mechanical properties of ultra-high-performance concrete incorporated with microencapsulated phase change material, Constr. Build. Mater. 273 (2021) 121714, https://doi.org/10.1016/j.conbuildmat.2020.121714.
[68] S. Drissi, K.H. Mo, A.C. Falchetto, T.C. Ling, Understanding the compressive strength degradation mechanism of cement-paste incorporating phase change material, Cem. Concr. Compos. 124 (2021), https://doi.org/10.1016/j.cemconcomp.2021.104249.
[69] A. Jayalath, R. San Nicolas, M. Sofi, R. Shanks, T. Ngo, L. Aye, P. Mendis, Properties of cementitious mortar and concrete containing micro-encapsulated phase change materials, Constr. Build. Mater. 120 (2016) 408–417, https://doi.org/10.1016/j.conbuildmat.2016.05.116.
[70] British Standards Institution (BSI), Methods of testing cement. Part 1, Determination of strength, BSI, 2016.
[71] S. Guo, Y. Wang, J. Zhang, L. Wu, Z. Song, Raman scattering spectroscopy study on chalcogenide phase-change materials, Mater. Sci. Eng. B 322 (2025) 118649, https://doi.org/10.1016/j.mseb.2025.118649.
[72] Z. Zhang, Z. Huang, C. Shi, Z. Wu, W. Zhang, P. Duan, Z. Jiang, Advancement in Raman spectroscopy (RS) for characterizing cementitious materials, J. Am. Ceram. Soc. 108 (2025) e20162, https://doi.org/10.1111/jace.20162.
[73] S.S. Potgieter-Vermaak, J.H. Potgieter, R. Van Grieken, The application of Raman spectrometry to investigate and characterize cement. Part I: A review, Cem. Concr. Res. 36 (2006) 656–662, https://doi.org/10.1016/j.cemconres.2005.09.008.
[74] K. Jiao, L. Lu, T. Wen, Q. Wang, A novel two-dimensional continuum mixture theory model for paraffin wax melting in a cavity heating from side considering volume change, J. Energy Storage 78 (2024), https://doi.org/10.1016/j.est.2023.110026.
[75] V.Z. Vargas, L.J. Claros-Marfil, G.F.B. Sandoval, B.Heredia Rojas, A.García Santos, F.J.Neila González, Experimental assessment of energy storage in microencapsulated paraffin PCM cement mortars, Case Stud. Constr. Mater. 20 (2024) e02959, https://doi.org/10.1016/j.cscm.2024.e02959.
[76] A. Jayalath, R. San Nicolas, M. Sofi, R. Shanks, T. Ngo, L. Aye, P. Mendis, Properties of cementitious mortar and concrete containing micro-encapsulated phase change materials, Constr. Build. Mater. 120 (2016) 408–417, https://doi.org/10.1016/j.conbuildmat.2016.05.116.
[77] M. Aguayo, S. Das, A. Maroli, N. Kabay, J.C.E. Mertens, S.D. Rajan, G. Sant, N. Chawla, N. Neithalath, The influence of microencapsulated phase change material (PCM) characteristics on the microstructure and strength of cementitious composites: Experiments and finite element simulations, Cem. Concr. Compos 73 (2016) 29–41, https://doi.org/10.1016/j.cemconcomp.2016.06.006.
[78] G.V.N. Trivedi, R. Parameshwaran, Cryogenic conditioning of microencapsulated phase change material for thermal energy storage, Sci. Rep. 10 (2020) 18353, https://doi.org/10.1038/s41598-020-75494-8.
[79] A. Vasu, F.Y. Hagos, M.M. Noor, R. Mamat, J. Kaur, The effect of thermal cyclic variation on the thermophysical property degradation of paraffin as a phase changing energy storage material, Appl. Therm. Eng. 149 (2019) 22–33, https://doi.org/10.1016/j.applthermaleng.2018.12.033.
[80] N. Hernandez, J. Lizarazo-Marriaga, M.A. Rivas, Petrographic characterization of Portlandite crystal sizes in cement pastes affected by different hydration environments, Constr. Build. Mater. 182 (2018) 541–549, https://doi.org/10.1016/j.conbuildmat.2018.06.142.
[81] L. Li, H. Yu, X. Wang, S. Zheng, Thermal analysis of melting and freezing processes of phase change materials (PCMs) based on dynamic DSC test, Energy Build. 130 (2016) 388–396, https://doi.org/10.1016/j.enbuild.2016.08.058.
[82] C. Politi, Algorithmic thermophysical analysis of composite PCM–perlite materials, using machine learning mechanisms, for optimizing passive energy storage in buildings, Doctoral thesis, National Technical University of Athens, 2025.
[83] A. Wadee, P. Walker, N. McCullen, V. Ferrandiz-Mas, The effect of thermal cycling on the thermal and chemical stability of paraffin phase change materials (PCMs) composites, Mater. Struct. 58 (2025) 25, https://doi.org/10.1617/s11527-024-02556-y.
[84] W.N. dos Santos, Effect of moisture and porosity on the thermal properties of a conventional refractory concrete, J. Eur. Ceram. Soc. 23 (2003) 745–755, https://doi.org/10.1016/S0955-2219(02)00158-9.
[85] M. Kraiem, M. Karkri, M. Fois, P. Sobolciak, Thermophysical characterization of paraffins versus temperature for thermal energy storage, Buildings 13 (2023) 877, https://doi.org/10.3390/buildings13040877.